Sr-isotope analysis of speleothems by LA-MC-ICP-MS: high temporal resolution and fast data acquisition

Michael Weber[1,2]*, Jasper A. Wassenburg[1,2], Klaus Peter Jochum[2], Sebastian F.M. Breitenbach[3], Jessica Oster[4], Denis Scholz[1]

[1]Institut für Geowissenschaften, Johannes Gutenberg-Universität Mainz, J.-J.-Becher-Weg 21, 55128 Mainz, Germany

[2]Climate Geochemistry Department, Max-Planck-Institute for Chemistry (Otto-Hahn-Institute), Postbox 3060, 55020 Mainz, Germany

[3]Sediment and Isotope Geology, Ruhr-Universität Bochum, Universitätsstrasse 150, 44801 Bochum, Germany

[4]Department of Earth and Environmental Science, Vanderbilt University, Nashville, TN, 37240, USA

*Corresponding author:
Michael Weber
Institute for Geosciences, University of Mainz, Johann-Joachim-Becher-Weg 21, 55128 Mainz, Germany
Email: mweber02@students.uni-mainz.de

Abstract

Speleothems are well established climate archives. A wide array of geochemical proxies, including stable isotopes and trace elements are present within speleothems to reconstruct past climate variability. However, each proxy is influenced by multiple factors, often hampering robust interpretation. Sr isotope ratios ($^{87}Sr/^{86}Sr$) can provide useful information about water residence time and water mixing in the host rock, as they are not fractionated during calcite precipitation. Laser ablation multi-collector-inductively coupled plasma mass spectrometry (LA-MC-ICP-MS) has rarely been used for determination of Sr isotope signatures in speleothems, as speleothems often do not possess appropriately high concentrations of Sr to facilitate this analysis. Yet the advantages of this approach include rapid data acquisition, higher spatial resolution, larger sample throughput and the absence of chemical treatment prior to analysis. We present LA-MC-ICP-MS Sr isotope data from two speleothems from Morocco (Grotte de Piste) and India (Mawmluh Cave), and we compare linescan and spot analysis ablation techniques along speleothem growth axes. The analytical uncertainty of our LA-MC-ICP-MS Sr data is comparable to studies conducted on other carbonate materials. The results of both ablation techniques are reproducible within analytical error, implying that this technique yields robust results when applied to speleothems. In addition, several comparative measurements of different carbonate reference materials (i.e. MACS-3, JCt-1, JCp-1), including tests with standard bracketing and comparison of the $^{87}Sr/^{86}Sr$ ratios with a nanosecond laser ablation system and a state-of-the-art femtosecond laser ablation system, highlight the robustness of the method.

Keywords: Speleothem; Strontium isotopes; Laser ablation, Multi-collector inductively coupled plasma mass spectrometry, Femtosecond

1. Introduction

Speleothems (cave $CaCO_3$ deposits) are well established climate archives and are found worldwide in karst environments (Asmerom et al., 2010; Cheng et al., 2016; Cruz et al., 2005; Genty et al., 2003; Hoffmann et al., 2016; Kennett et al., 2012; Luetscher et al., 2015; Wang et al., 2001). They can be dated with unprecedented precision using the ^{230}Th/U-dating method (Richards and Dorale, 2003; Scholz and Hoffmann, 2008), and provide a range of climate proxies that record a number of environmental processes and can be analysed at up to sub-annual resolution.

Oxygen isotopes in speleothems ($\delta^{18}O$ values) depend on paleo-temperature and rainfall properties, such as amount, seasonality and moisture sources (e.g., Fairchild et al., 2006; McDermott, 2004), whereas carbon isotopes can provide information on soil productivity, vegetation characteristics and effective rainfall (McDermott, 2004). In addition, trace elements (e.g., Sr, Mg, P, Ba) may be interpreted in terms of effective infiltration, prior calcite precipitation, water residence time, source and reservoir effects, weathering processes in the epikarst zone and soil composition (Ayalon et al., 1999; Fairchild et al., 2000; Fairchild and Treble, 2009; Verheyden et al., 2000; Wassenburg et al., 2016a; Wassenburg et al., 2016b). Within the epikarst and soil zone, different sources of trace elements (for example aeolian dust vs. host rock) may be present and display varying compositions. A change in the dripwater pathway or in the relative contribution of different sources, may thus affect the dripwater trace element composition, which often renders their interpretation a challenging task (Banner et al., 1994).

Important information on the influence of different sources of trace elements in dripwaters may be provided by Sr isotopes, which have been shown to provide additional insights on precipitation and water residence time in the host rock (Banner et al., 1996; Oster et al., 2010). In $CaCO_3$, the Sr^{2+} ion substitutes at the Ca^{2+} ion sites in the mineral lattices due to their similar

77 properties and ionic radii (Banner, 2004). No isotopic fractionation of Sr isotopes is observed
78 during precipitation of $CaCO_3$ and the incorporation of Sr into the crystal lattice. Thus, the
79 $^{87}Sr/^{86}Sr$ ratio of carbonates is identical to that of the parent solution (Banner and Kaufman,
80 1994).

81 Although the first Sr isotope analyses on speleothems were conducted in 1990 (Avigour et al.,
82 1990), relatively few studies have focused on this topic so far. The main source for Sr in
83 speleothems is the host rock, but several factors have been proposed to affect Sr isotope ratios:
84 varying water residence time in the epikarst (Banner et al., 1996); (Oster et al., 2010; Oster et
85 al., 2014; Verheyden et al., 2000), changes in aeolian input in response to sea-level changes or
86 atmospheric circulation (Goede et al. 1998; Ayalon et al. (1999); Bar-Matthews et al. (1999);
87 Li et al. (2005); Zhou et al. 2009), changes in weathering intensity of soil and host rock in
88 response to rainfall (Avigour et al., 1990), changes in the distance to the shoreline and
89 incorporation of sea-salt signals (Fisher et al., 2010), as well as mixing of the Sr signals of
90 different rock types and soils (Frumkin and Stein (2004); Hori et al. (2013). All these studies
91 either used Thermal Ionization Mass Spectrometry (TIMS, Avigour et al. (1990); Goede et al.
92 (1998); Frumkin and Stein (2004); Li et al. (2005); Zhou et al. (2009); Hori et al. (2013)), or
93 solution MC-ICP-MS (multi-collector inductively coupled plasma mass spectrometry, Ayalon
94 et al. (1999); Bar-Matthews et al. (1999); Verheyden et al. (2000); Fisher et al. (2010); (Oster
95 et al., 2010; Oster et al., 2014). For both techniques samples need to be drilled/milled, and
96 require chemical separation prior to mass spectrometric analysis. This is time-consuming, and
97 limits the achievable spatial resolution of $^{87}Sr/^{86}Sr$ records. Strontium isotope analysis by laser
98 ablation (LA-) MC-ICP-MS offers the opportunity to measure the $^{87}Sr/^{86}Sr$ ratio *in-situ* at high
99 spatial resolution and without any prior chemical treatment. Although this technique has been
100 widely applied to petrological samples (e.g. Christensen et al. (1995); Davidson et al. (2001);
101 Waight et al. (2002); Bizzarro et al. (2003); Ramos et al. (2004); Jackson and Hart (2006), and

carbonate and phosphate materials, such as gastropods, otoliths, teeth, clam shells, fine- and coarse-grained carbonates and corals (Christensen et al. (1995), Ehrlich et al., 2001, Outridge et al. (2002), Bizzarro et al., 2003, Ramos et al., 2004, Woodhead et al. (2005), Copeland et al. (2008), it has only recently been used for measuring $^{87}Sr/^{86}Sr$ in speleothems (Wortham et al., 2017).

Here we present a LA-MC-ICP-MS method for measuring Sr isotopes on speleothems, based on previously mentioned studies on different sample materials. We show results from two speleothem samples and compare different sampling techniques. Both samples consist of aragonite and have a rather high Sr concentration >300 µg/g, which makes them highly suitable to apply LA-MC-ICP-MS. We also discuss the effects of different tuning parameters and compare results obtained by two different laser systems (a New Wave UP 213 nm laser and a NWR Femto200 laser ablation system).

2. Speleothem samples

The investigated speleothem samples stem from two different caves. Stalagmite GP5 was sampled at Grotte de Piste (Morocco), and stalagmite MAW-4 stems from Mawmluh Cave (Meghalaya, India). Stalagmite GP5 has a total length of 78 cm. A detailed description of the cave and the sample is given in Wassenburg et al. (2012) and Wassenburg et al. (2013). In this study, an approximately 15 cm long part of the sample (Fig. 1) was studied which corresponds to the time span from ca. 800 to 1760 AD. Previous data is published in Wassenburg et al. (2013) and only briefly summarised here. GP5 was precisely dated by the $^{230}Th/U$-method. Furthermore, the mineralogy of the sample was investigated by XRD and showed that GP5 is mainly aragonitic, with minor calcitic parts (<2%). Strontium concentrations range from 200 to

500 µg/g, with an average concentration of 426 (±49) µg/g. In some parts, the sample is characterized by mm-scale layering of porous and less porous layers.

Stalagmite MAW-4 (Fig. 1) from Mawmluh cave is a small sample with a total length of 3 cm. The upper part of the sample (~ 15 mm), consists of aragonite, and covers the time span from 1950 to 2006 AD (Wassenburg et al., 2016b). It has an average growth rate of ~293 µm/a, and can thus provide very high resolution. The stalagmite was actively growing at the time of collection (March 2006). The lower part of the sample consists of calcite, the base is dated 395 ± 55 a BP. The calcite-to-aragonite transition is clearly visible by a change in colour from greyish (calcite) to white/beige (aragonite). In the upper aragonitic part, this stalagmite has a relatively high Sr concentration (1458–1729 µg/g, (Wassenburg et al., 2016b), and is thus extremely suitable for Sr isotope measurements by LA-MC-ICP-MS. The calcite section has a Sr concentration of a few hundred µg/g, and was not investigated in this study. For more information about the cave setting and microclimatic conditions, see Breitenbach et al. (2010) and Breitenbach et al. (2015).

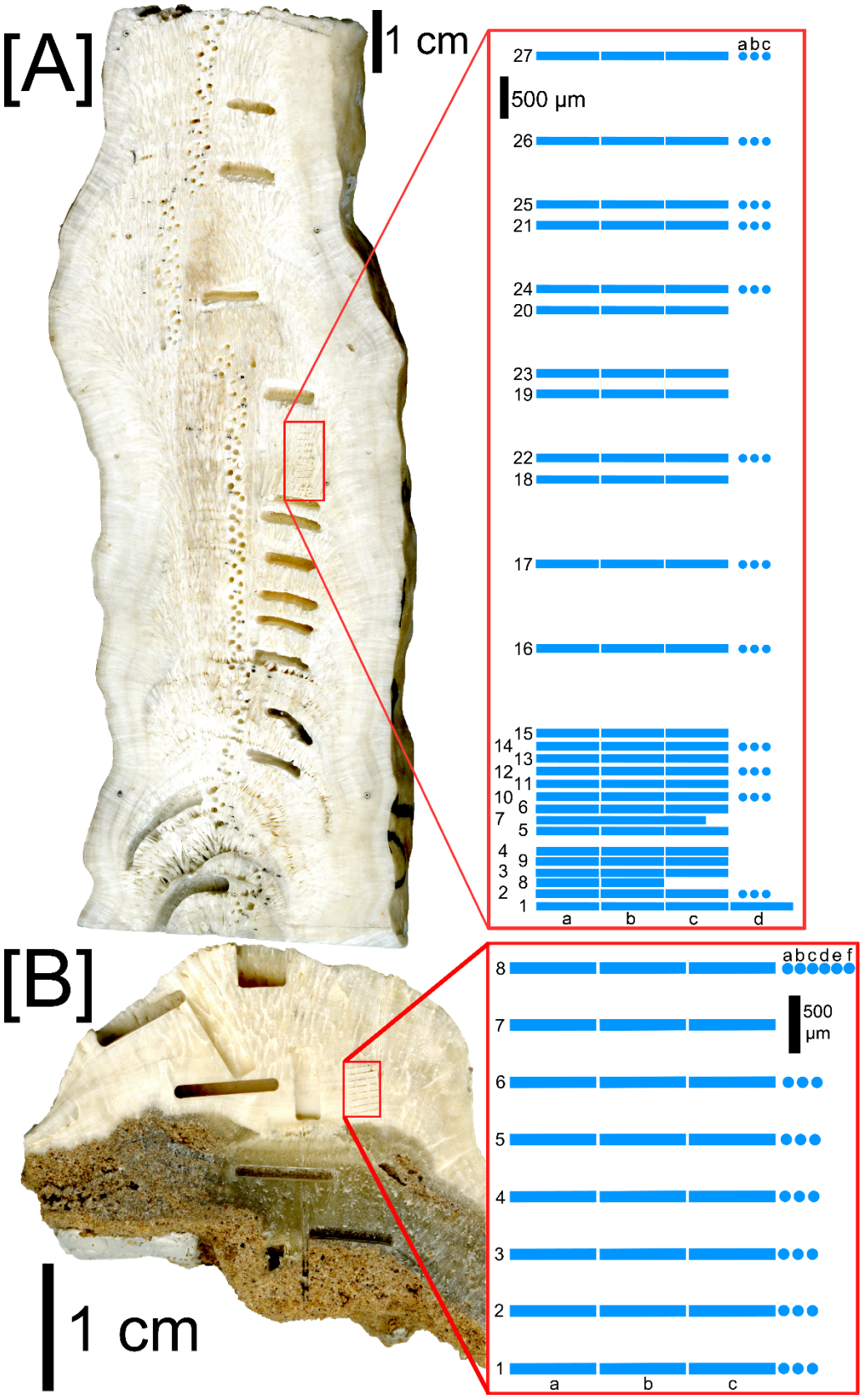

Figure 1: [A] Sampling approach for speleothem GP5. The red rectangle indicates the sampling section, blue lines show the LA-MC-ICP-MS linescan positions. The spot analyses were

142 performed near the right end of the third linescan as indicated by the blue spots. **[B]** Sampling
143 approach for speleothem MAW-4. The red rectangle indicates the sampling section. Linescan
144 and spot analyses are similarly indicated as in [A]. All line lengths, widths and distances are on
145 scale.

146

147 **3. Materials and methods**

148 **3.1 Analytical setups**

149 The measurement routine was developed with a NU Plasma MC-ICP-MS (see Table 1 for cup-
150 configuration) coupled with a New Wave UP213 nm Nd:YAG laser ablation system at the Max
151 Planck Institute for Chemistry, Mainz. Measurements were also performed with the MC-ICP-
152 MS coupled to a NWR Femto200 laser ablation system to compare results obtained with two
153 laser ablation systems. The femtosecond laser is less sensitive to matrix effects that may cause
154 isotope fractionation (Poitrasson et al., 2003; Vanhaecke et al., 2010). Prior to laser ablation,
155 the MC-ICP-MS was coupled to a CETAC Aridus II Desolvating Nebulizer system for tuning.
156 The Sr reference solution NIST SRM 987 was used for optimizing the peak shape and
157 coincidence of the individual Sr isotopes (^{88}Sr, ^{87}Sr, ^{86}Sr, ^{84}Sr) and to test the influence of
158 different tuning parameters on ion beam intensity and the $^{87}Sr/^{86}Sr$ ratio. Several tuning
159 parameters were changed systematically. Tests showed that the gas flows of the Aridus
160 introduction system have a significant effect on the Sr isotope ratios. Furthermore, the torch
161 position and the tuning of the high voltage lenses are important, since they affect the sample
162 introduction into the system and the ion beam inside the mass spectrometer. Finally, the source
163 lenses have been shown to have a significant effect on the $^{87}Sr/^{86}Sr$ ratio. In order to test the
164 effects of changes in the lens settings, we started with seven measurements of NIST SRM 987
165 to test the stability of the $^{87}Sr/^{86}Sr$ ratio over time. In a first step, the lens settings were tuned

for maximum ^{88}Sr intensity. Subsequently, the different source and transfer lens settings were changed systematically. For each lens, three measurements were performed: First, the voltage of the lens was decreased by 10 V, then increased by 20 V, and finally decreased by 10 V to return to the original value. This procedure was performed for all seven source and transfer lenses. Results are presented in Fig. 2 and Supplement A1.

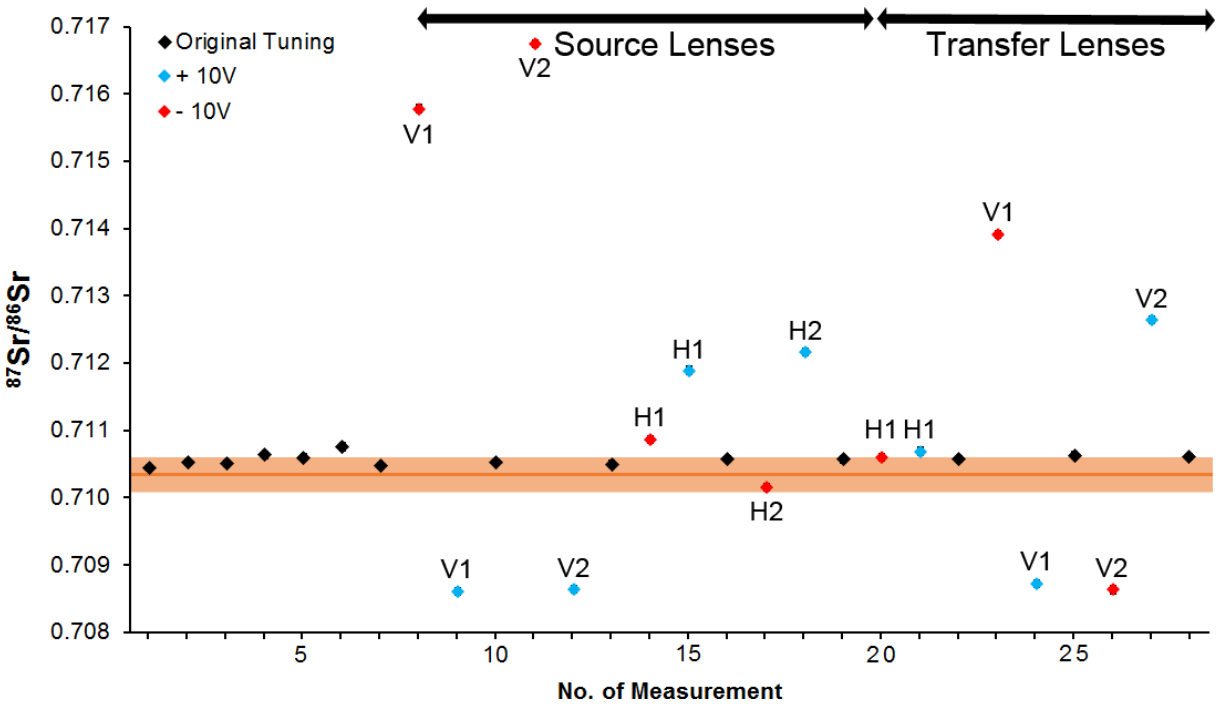

Figure 2: $^{87}Sr/^{86}Sr$ ratios obtained on reference solution NIST SRM 987. The orange line represents the literature value of $^{87}Sr/^{86}Sr = 0.71034 \pm 0.00026$ (GeoReM, (Jochum et al., 2005), the shading in bright orange shows the 2σ standard error. The large fluctuations in the Sr isotope ratio are caused by changes in the settings of the source and transfer lenses of the NU Plasma MC-ICP-MS, marked by the black arrows. Black diamonds represent measurements with the original lens settings, while blue (red) diamonds represent measurements with a 10 V increase (decrease) in lens voltage in comparison to the original lens setting.

Settings were then further optimised with the NU MC-ICP-MS coupled to the LA system. Since the UP213 nm laser ablation system offers higher fluence values (20 – 30 J/cm^2)and count rates than the femtosecond laser (0.7 – 0.8 J/cm^2), this system allows measurement of samples with comparably low Sr concentrations (>200 µg/g). Potential matrix effects are assessed by comparison with the femtosecond laser. All samples and reference materials have a low Rb content (Table 2). The operating parameters for the MC-ICP-MS and the laser ablation systems are given in Table 3.

3.2. Reference materials

The reference material (RM) JCt-1 was measured to determine the accuracy and precision of the method. This modern marine carbonate sample originates from a recent giant clam and has a $^{87}Sr/^{86}Sr$-ratio comparable to modern sea water ($^{87}Sr/^{86}Sr$ of 0.70918 ± 0.00001, 2σ, Faure and Mensing (2005)), as confirmed by solution MC-ICP-MS measurements ($^{87}Sr/^{86}Sr$ = 0.70915 ± 0.00005, Ohno and Hirata (2007). Recently, a more precise $^{87}Sr/^{86}Sr$ ratio of 0.70917 ± 0.00001 has been obtained for JCt-1 by MC-ICP-MS (Weber et al., In Revision). Due to its comparable Sr content of 1400 µg/g (Aizawa, 2008), JCt-1 was chosen as RM for the measurements of samples GP5 and MAW-4. Furthermore, the RMs JCp-1, a modern coral with $^{87}Sr/^{86}Sr$ = 0.70916 ± 0.00002 (Ohno and Hirata (2007)) and MACS-3, a synthetic carbonate pellet ($^{87}Sr/^{86}Sr$ = 0.7075532 ± 0.0000037; Jochum et al. (2011)), were also tested. Both of these RM samples have a very high Sr concentration (7500 µg/g for JCp-1, (Aizawa, 2008), and 6760 µg/g for MACS-3, (Jochum et al., 2012) and are well suited for femtosecond laser analysis. For tuning and test measurements, we used a modern day bivalve shell of *Glycimeris* sp., which has two distinct areas of different Sr concentrations of ca. 1000 and 5000 µg/g.

3.3. Laser ablation sampling method

Multiple LA-MC-ICP-MS measurements were performed perpendicular to the growth axis of the speleothem samples, parallel to and within the same distinct growth layers to check for reproducibility. In order to identify the best method for analysing Sr-isotope ratios in speleothems by LA-MC-ICP-MS, we applied two different sampling methods. First, we used the linescan technique, which has the advantage that a high signal intensity can be maintained for a relatively long measurement interval, improving counting statistics. In contrast, for spot analyses, the signal intensity slowly decreases with ablation depth. However, for spot analyses, mixing of material from different growth layers is excluded. The linescans followed individual growth bands and each of usually three linescans per growth layer had a circular spot size of 80 – 100 µm and a length of 750 µm (except linescan GP5-7, which was 2000 µm). They were scanned with a scan-speed of 5 µm/s, providing about 150 s per linescan measurement. This sampling approach enables us to identify potential changes in the $^{87}Sr/^{86}Sr$ ratio at a very high spatial resolution. Prior to each analysis, a pre-ablation was performed with a spot size of 110 µm and a scan-speed of 80 µm/s (Table 3). The first 5 s are discarded due to high intensities when the laser starts, which is typical for laser ablation analyses. Spots were analysed with a circular spot size of 100 µm and a dwell time of 120 s. To test the reproducibility of the method, three line scans were placed parallel to each other within the same growth band with less than 50 µm between the end and start of each linescan (Fig. 1). The distance between the measured layers varied between 150 µm and 850 µm for GP5 and 500 µm for MAW-4. The spot analyses of GP5 were performed for a few layers only. Each spot analysis is located near the end of the respective line scan. For correction purposes, RM JCt-1 was measured three times before and after each set of samples (usually six measurements in total).

To compare both laser ablation systems, we performed measurements with different RMs. Since the Sr concentration of JCp-1 is almost six times that of JCt-1, the laser settings for the

UP213 laser ablation system were adjusted to prevent the ^{88}Sr intensity from reaching critical values. We used a laser energy of 60 %, a repetition rate of 5 Hz and a spot size of 55 µm. All measurements were performed as spot analyses. To test the robustness of the results, we also applied our standard bracketing approach on JCp-1 by measuring samples of JCt-1 before and after JCp-1. The laser settings for JCt-1 were chosen as described in Table 3.

Our NWR Femto200 laser ablation system only allows spot sizes up to 65 µm, therefore we only measured RMs with high Sr concentrations, such as JCp-1 and MACS-3. The laser parameters for these measurements are presented in Table 3. Spot measurements with the femtosecond laser ablation system suffer from a rapid decrease in signal intensity. Thus, all measurements were performed as linescans. We measured three samples of JCp-1, followed by six measurements of MACS-3 and again three samples of JCp-1.

4. Correction procedure for LA-MC-ICP-MS

Strontium isotopes were measured on cups H4 (^{88}Sr), H2 (^{87}Sr), Ax (^{86}Sr) and L3 (^{84}Sr) (Table 1). The major advantage of Sr-isotope analysis with LA-MC-ICP-MS is that Sr-isotopes are measured *in-situ*, without the need of chemical separation. This means, however, that the matrix contains several other isotopes that potentially affect the Sr isotope signal (i.e., ^{87}Rb, but also doubly charged ions, such as ^{176}Yb, ^{174}Yb, ^{172}Yb, ^{168}Yb, ^{168}Er, and molecular interferences, such as Ca-argides and/or -dimers, Table 1). In addition, the Ar gas may contain impurities of Kr, with interfering isotopes of ^{86}Kr and ^{84}Kr (Table 1). Some masses are affected by several interferences. For example, the ^{84}Sr signal on mass 84 may be affected by $^{84}Kr^{+}$, $^{168}Er^{2+}$ $^{168}Yb^{2+}$ and Ca argides/dimers. Therefore, it is necessary to find another mass that is not affected by other interferences, which can be used to correct for other masses of the same ion using known isotopic abundances. For example, we used mass number 86.5 that is mostly unaffected by other

signals to correct for the Yb-interference by monitoring $^{173}Yb^{2+}$. Thus, the order of the corrections is important. The correction procedure is outlined in detail below. Fig. 3 shows the magnitude of the individual correction steps on the $^{87}Sr/^{86}Sr$ ratio for measurements on samples JCt, GP5 and MAW-4.

4.1 Background correction

Potential interferences of ^{86}Kr, ^{84}Kr, ^{83}Kr and ^{82}Kr from minor contaminations in the Ar gas supply are corrected by a blank measurement. For this reason, prior to each analysis an on-peak background correction is performed for 45 s during the laser warm-up time. Then, the median for each signal intensity is calculated and subtracted from the measured signal. This removes all Kr interferences as well as potential remains of Sr from previous measurements.

4.2 Rare-earth elements (REE)

After background correction, different interferences must be eliminated. Doubly-charged isotopes of Er and Yb can be detected on half masses (Table 1). ^{173}Yb is the only isotope measured on cup H1 on half-mass 87.5, and ^{171}Yb is the only one measured on cup L1 on half mass 85.5. Thus, ^{173}Yb and ^{171}Yb can be measured without any interferences. By assuming constant isotope ratios for Yb (Berglund and Wieser (2011), the signal for all Yb isotopes can be calculated. Although Yb is quite rare in speleothem samples (Table 2), this correction may have a minor influence on the $^{87}Sr/^{86}Sr$ ratios.

The second step is to correct for Er. ^{167}Er is the only isotope measured on ion counter IC-1 on half mass 83.5, and other Er isotopes can be calculated assuming constant isotope ratios in the same way as Yb (Berglund and Wieser (2011). Erbium is uncommon in speleothem samples (Table 2) and this correction is only of minor importance. Several laser ablation studies on other

sample materials did not even correct for rare earth elements (REE) during Sr isotope analysis (e.g. Christensen et al. (1995); Barnett-Johnson et al. (2005); Jochum et al. (2009); Copeland et al. (2010)).

4.3 Molecular interferences

The next step is to correct for molecular interferences of Ca dimers and argides. Since it is impossible to differentiate between the signals resulting from argides and dimers, the relative amounts of each signal are taken into account to correct for those interferences in relation to the signal on mass 82. This mass is used as a reference since it has no other interferences and a potentially higher signal of argides and dimers than mass 83, which is also free of significant interferences (Table 1). As an example, we briefly describe the correction of mass 84 for Ca argides and dimers.

After correcting for background and REEs, the correction for Ca argides is performed by the following relationship:

$$84_{ArCorr} = 84_{uncorr} - 82_{uncorr} * \left({\sum \mathrm{CaAr}_{84}} \Big/ {\sum \mathrm{CaAr}_{82}} \right) \quad \text{(Eq. 1)}$$

where 84_{ArCorr} is the corrected signal on mass 84, 84_{uncorr} is the uncorrected signal (besides background and REE correction) on mass 84 and 82_{uncorr} is the signal on mass 82. $\Sigma CaAr_{84}$ is the sum of the relative portion of Ca argides on mass 84, and $\Sigma CaAr_{82}$ is the sum of the relative portion of Ca argides on mass 82, based on their natural occurrence (Berglund and Wieser, 2011). This correction is performed for masses 88, 86, 84 and 83. For the interferences from Ca dimers, the correction is done in a similar way, again using the signal on mass 82 as a reference:

$$84_{Corr} = 84_{ArCorr} - 82_{uncorr} * \left({\sum \mathrm{CaCa}_{84}} \Big/ {\sum \mathrm{CaCa}_{82}} \right) \quad \text{(Eq. 2)}$$

where 84_{Corr} is the corrected signal on mass 84, 84_{Arcorr} is the background corrected intensity on mass 84, REEs and Ca argides, and 82_{uncorr} is the uncorrected signal (besides background and REE correction) on mass 82. $\Sigma CaCa_{84}$ is the sum of the relative portion of Ca dimers on mass 84 and $\Sigma CaCa_{82}$ is the sum of the relative portion of Ca dimers on mass 82. This correction is performed for masses 88, 87, 86, 85, 84 and 83 and only applied for signals > 0 V. All other signals remain uncorrected because the intensity of Ca argides and dimers is too small to detect and does not affect the results.

4.4 Mass bias

After correcting the raw signals for interferences, the mass bias needs to be corrected. This correction is performed prior to the correction for the interference of Rb, because the mass bias obtained from the $^{86}Sr/^{88}Sr$ ratio is subsequently used to obtain the mass bias corrected $^{85}Rb/^{87}Rb$ ratio (section 4.5). Based on the signals corrected for background, REEs, Ca argides and dimers, raw values for the ratios of $^{86}Sr/^{88}Sr$, $^{84}Sr/^{86}Sr$ and $^{87}Sr/^{86}Sr$ are calculated. Then, a mass fractionation factor α is calculated to correct for the instrumental mass fractionation based on the $^{86}Sr/^{88}Sr$ ratio and the exponential law described in Ingle et al. (2003):

$$R_{corr} = R_{meas} * \left({}^{m_{87Sr}}/_{m_{86Sr}}\right)^{\alpha} \quad \text{(Eq. 3)}$$

where m_{87} and m_{86} are the masses of ^{87}Sr and ^{86}Sr. The mass fractionation factor α is calculated as described in Ehrlich et al. (2001):

$$\alpha = \left(ln \frac{\left({}^{86Sr}/_{88Sr}\right)_{true}}{\left({}^{86Sr}/_{88Sr}\right)_{meas}} \right) \Big/ ln\left({}^{m_{86}}/_{m_{88}}\right) \quad \text{(Eq. 4)}$$

where $(^{86}Sr/^{88}Sr)_{true}$ is the accepted value of 0.1194 (Steiger and Jäger, 1977) and m_{88} is the mass of ^{88}Sr.

4.5 Interference of rubidium

The final step in the correction procedure is to correct the $^{87}Sr/^{86}Sr$ ratio for the interference of ^{87}Rb. Due to the previous corrections, mass 85 only consists of ^{85}Rb (Table 1), which can be used to calculate the fraction of ^{87}Rb by using the constant ratio of $^{87}Rb/^{85}Rb = 0.3857$ (Berglund and Wieser (2011) This was done following equation 5:

$$^{87}Rb = \left({}^{87}Rb \Big/ {}_{85}Rb_{Lit} * {}^{85}Rb_{meas} \right) * \left(m_{87} / m_{85} \right)^{\alpha} \quad \text{(Eq. 5)}$$

where $^{87}Rb/^{85}Rb_{Lit}$ is the literature value (Berglund and Wieser, 2011)(Berglund and Wieser, 2011)(Berglund and Wieser, 2011), $^{85}Rb_{meas}$ is the Rb signal on mass 85, corrected for background, REEs and Ca argides/dimers, m_{87} is the mass of ^{87}Rb, m_{85} is the mass of ^{85}Rb, and α is the mass fractionation factor. The correction on $^{87}Sr/^{86}Sr$ is then performed using the following equation:

$$^{87}Sr \Big/ {}_{86}Sr_{RbCorr} = \left[\left({}^{87}Sr_{uncorr} - {}^{87}Rb \right) \Big/ {}_{86}Sr \right] * \left(m_{87} / m_{86} \right)^{\alpha} \quad \text{(Eq. 6)}$$

where $^{87}Sr_{uncorr}$ is the Sr signal on mass 87 corrected for background, REEs and argides/dimers (not for Rb), ^{87}Rb and ^{86}Sr are the corrected signals for Rb on mass 87 and Sr on mass 86, respectively, m_{87} and m_{86} are the masses for Sr and α is the mass fractionation factor. This Rb correction is only considered robust for samples with a Rb/Sr ratio <0.02 (Irrgeher et al., 2016). For samples with higher Rb content, an alternative Rb-correction is necessary (Müller and Anczkiewicz, 2016). All speleothem samples and RMs analysed in this study are below this threshold (Table 2).

4.6 Data processing

After calculating the interference-free $^{87}Sr/^{86}Sr$ ratio, the results are calibrated by standard-bracketing using RMs with well-known $^{87}Sr/^{86}Sr$ ratios, as has been recommended for Sr-isotope analysis (Irrgeher et al., 2016). Furthermore, to avoid effects of individual large peak values, we performed a 2σ outlier test for the median of all $^{87}Sr/^{86}Sr$ values, removing all values deviating >2σ from the median.

Usually, the final $^{87}Sr/^{86}Sr$ ratios obtained for the RMs deviate slightly from the reference values, necessitating an additional correction step. Each sample is therefore bracketed by a set of three individual measurements of a suitable RM. The mean value of the three RMs is calculated, and a correction factor for the sample is calculated according to the following equation:

$$Sr_{Corr} = \frac{{}^{87}Sr/_{{}^{86}Sr_{true}}}{{}^{87}Sr/_{{}^{86}Sr_{meas}}} \quad \text{(Eq. 7)}$$

where $^{87}Sr/^{86}Sr_{true}$ is the literature value of the RM and $^{87}Sr/^{86}Sr_{meas}$ is the measured ratio of the RM. We then use the mean value of the two correction factors from the two sets of RMs (measured prior and subsequent to the sample) and apply it to the measured sample $^{87}Sr/^{86}Sr$ ratio. Since the measurements of the RMs are associated with an uncertainty, error propagation is performed by adding the relative 2σ standard error for the measurement of the RM (2σ Std Err_{Ref}) to the relative 2σ standard error of the measured sample (2σ Std Err_{Spl}):

$$2\sigma\ Std\ Err_{SampleCorr}[\%] = \sqrt{\left(2\sigma\ Std\ Err_{Ref}[\%]\right)^2 + \left(2\sigma\ Std\ Err_{Spl}[\%]\right)^2} \quad \text{(Eq. 8)}$$

The 2σ Std Err_{Ref} value is calculated from the mean of the relative 2σ standard errors of all RMs, while the 2σ Std Err_{Spl} is calculated from the mean of the linescans or spot measurements for each sample layer. By applying the error propagation, the 2σ standard error of each sample usually increases by ± 0.00001 – 0.00002 (0.01 – 0.03 ‰).

5. Results

The results from the speleothem samples obtained with the two sampling methods (linescans and spot analyses, respectively) are presented in Table 2. Due to the extensive correction procedure, we show the effect of each correction step on the $^{87}Sr/^{86}Sr$ value for one LA-MC-ICP-MS measurement of JCt-1, MAW-4 and GP5, respectively. The results are presented in Fig. 3. The correction step associated with the largest effect is the background correction and, depending on the sample, the corrections for interferences of Yb and Rb. Corrections for Ca argides and dimers are insignificant for our results.

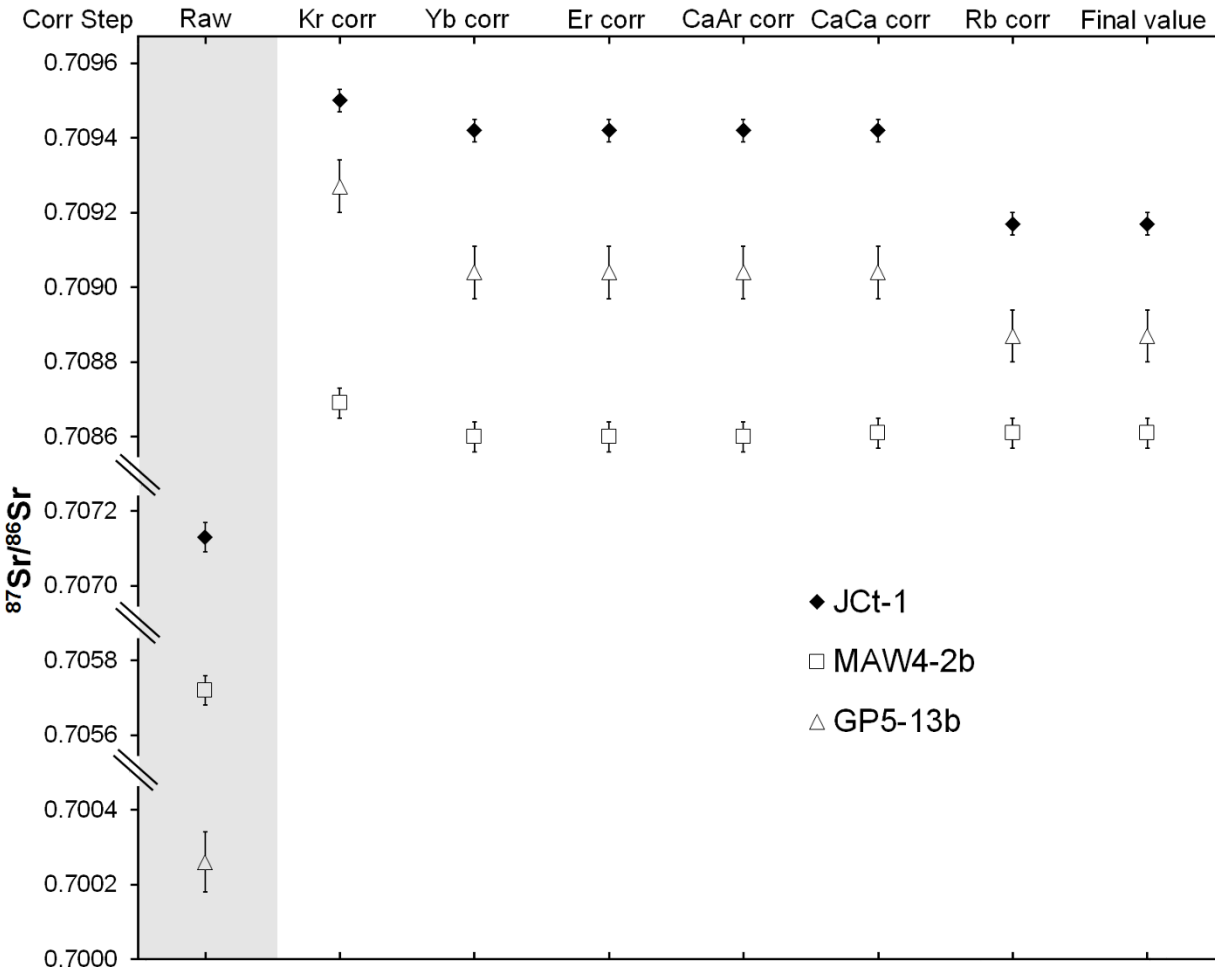

Figure 3: Influence of the different correction steps on the $^{87}Sr/^{86}Sr$ ratio of JCt-1 (black diamonds), MAW-4 (squares) and GP5 (triangles). Note that all results are mass bias corrected.

5.1. Influence of tuning parameters on the $^{87}Sr/^{86}Sr$ ratio

Our solution MC-ICP-MS measurements show that tuning for maximum Sr intensity does not necessarily lead to a "true" $^{87}Sr/^{86}Sr$ ratio, but may deviate from the accepted value of the reference solution NIST SRM 987 ($^{87}Sr/^{86}Sr$ = 0.71034 ± 0.00026, GeoReM, Jochum et al. (2005)) on the third or fourth decimal. This can be avoided by tuning the mass spectrometer to obtain the Sr isotope ratio known from the literature (at the expense of signal intensity). The procedure is described in chapter 3.1. While some changes have a large influence on the isotope ratio (e.g. the decrease by 10 V for source lenses V1 and V2), others only have a minor influence, such as the changes at transfer lens H1 (Fig. 2). We note that this might be a specific pattern for our mass spectrometer and may differ in other laboratories. After restoring to the original setting, the $^{87}Sr/^{86}Sr$ ratio was comparable to the starting value (Fig. 2).

Figure 4 (data in Supplement A1) shows the evolution of the $^{87}Sr/^{86}Sr$ ratio during consecutive days of LA-MC-ICP-MS measurements of RM JCt-1. While the Sr isotope ratio increased during the first measurements, source lens adjustments brought the $^{87}Sr/^{86}Sr$ ratio back towards the reference value.

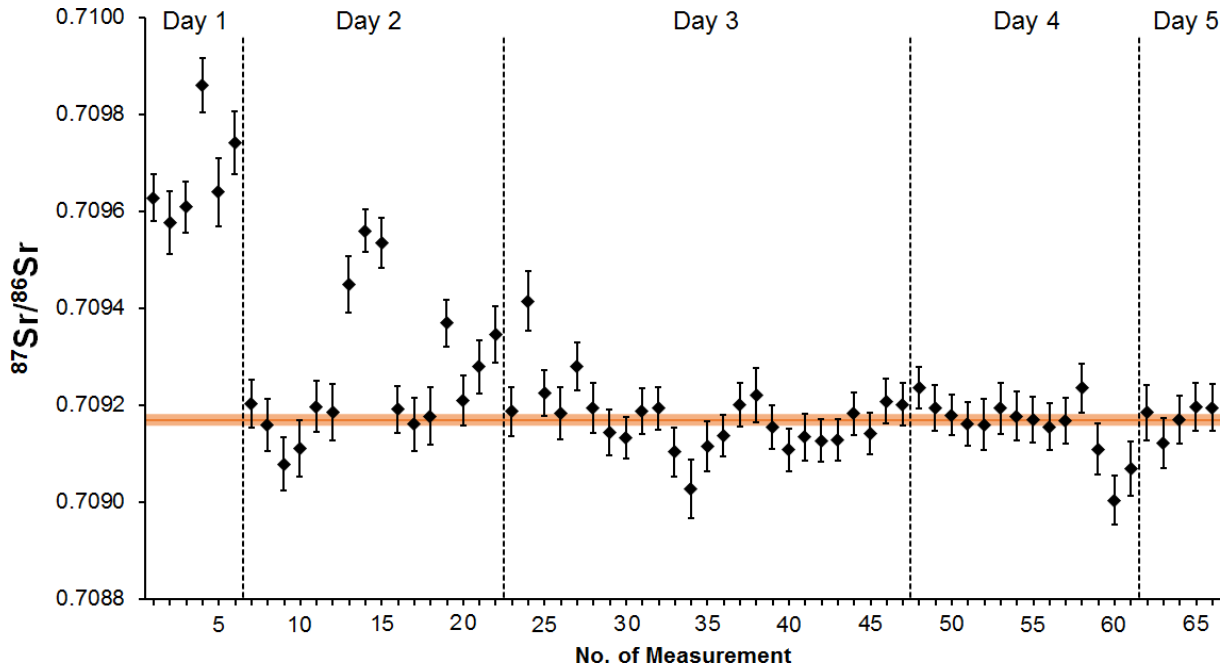

Figure 4: $^{87}Sr/^{86}Sr$ ratios of reference material JCt-1 obtained during different days, showing the tuning influence during the first measurements. The orange line represents the reference value of JCt-1 of $^{87}Sr/^{86}Sr = 0.70917 \pm 0.00001$ (Weber et al., In Revision), the shading in bright orange corresponds to its 2σ standard error. Dashed vertical lines separate different days of measurements. (For interpretation of the references to colour in this figure legend, the reader is referred to the web version of this article.)

These results highlight the necessity of the standard-bracketing approach, which corrects the described effects. Nevertheless, we minimised the influence of these effects by tuning the $^{87}Sr/^{86}Sr$ ratio towards the reference value prior to the measurement, or, if necessary, again afterwards.

5.2 Tests with reference materials

5.2.1 Nanosecond LA-MC-ICP-MS

For the nanosecond laser ablation system, we chose the carbonate RMs JCt-1, JCp-1 and MACS-3 and applied the method described above (section 3.3). These RM's have a large range of Sr concentrations, and we are aware that changes of the laser parameters between different samples can affect the measurements. Nevertheless, all measurements showed sufficient fluence (~ 10 J/cm^2 for JCp-1 and MACS-3 and > 22 J/cm^2 for JCt-1) and the obtained $^{87}Sr/^{86}Sr$ ratios showed the expected results within error. The mean value of the JCp-1 measurements was $^{87}Sr/^{86}Sr$ = 0.70913 ± 0.00008 (n = 3) and agree with the literature value of 0.70916 ± 0.00002 (Ohno and Hirata, 2007). In addition, the uncorrected JCp-1 $^{87}Sr/^{86}Sr$ ratio is 0.70914 ± 0.00007 (n = 3) and the uncorrected $^{87}Sr/^{86}Sr$ ratio of JCt-1 is 0.70917 ± 0.00005 (n = 5), thus both are indistinguishable from the literature values. The results for MACS-3 provide an average $^{87}Sr/^{86}Sr$ value of 0.70753 ± 0.00005 (n = 16), which is in agreement with the literature value of 0.7075532 ± 0.0000037 (Jochum et al., 2011).

5.2.2 Femtosecond LA-MC-ICP-MS

In order to further test our methodology, we used a femtosecond laser ablation system on carbonate RM's with high Sr concentrations (JCp-1 and MACS3) following the method as described in chapter 3.3. All measurements were corrected by the standard bracketing approach yielding $^{87}Sr/^{86}Sr$ ratios in agreement with the reference values (Fig. 5). An exception is measurement MACS-3-8, which shows a strongly elevated $^{87}Sr/^{86}Sr$ ratio. This sample may have been affected by changes in the Kr signal intensity because unusual peak intensities in ^{84}Kr were observed during the blank measurement. It is thus likely that similar fluctuations occurred during the measurement which affected the $^{87}Sr/^{86}Sr$ ratio. The measured raw $^{87}Sr/^{86}Sr$ ratios before the standard bracketing correction for JCp-1 are 0.70920 ± 0.00004 (n = 6) and 0.70757 ± 0.00005 for MACS-3 (without MACS3-8, n = 5), in agreement with the literature values. After performing the standard bracketing approach, the average $^{87}Sr/^{86}Sr$ ratio is

0.70917 ± 0.00006 for JCp-1 (n = 6) and 0.70752 ± 0.00006 for MACS-3 (without MACS3-8, n = 5).

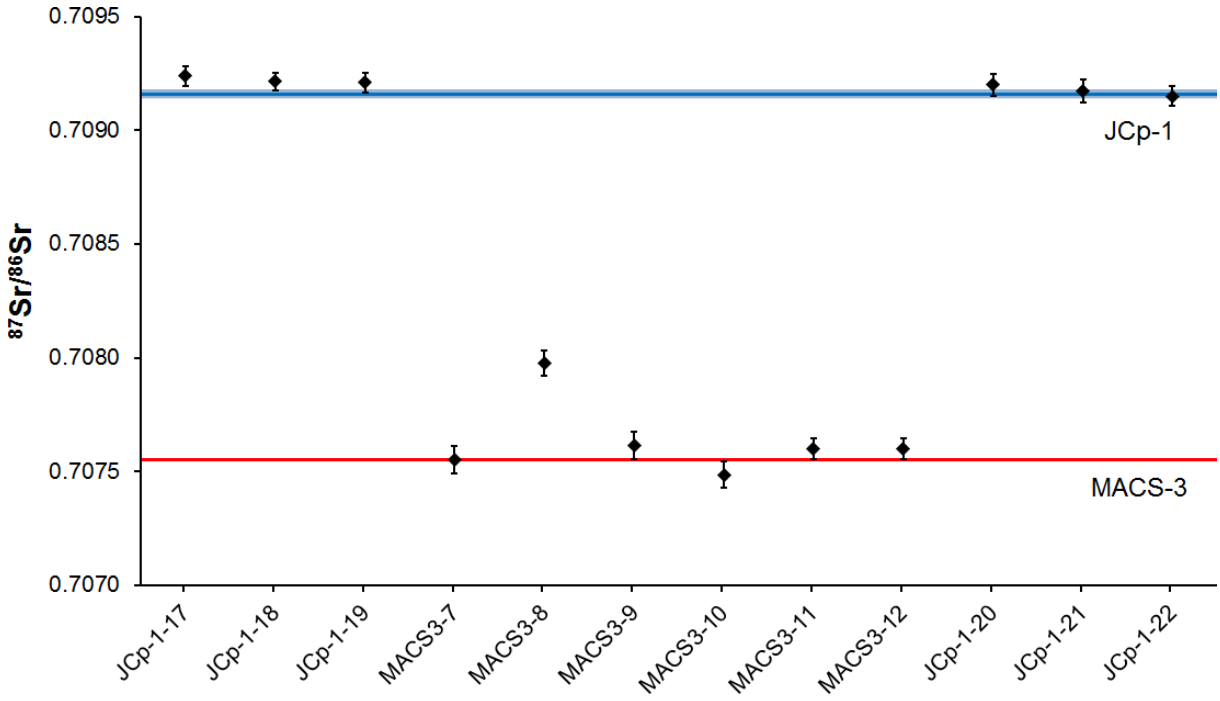

Figure 5: $^{87}Sr/^{86}Sr$ ratios of reference materials JCp-1 and MACS-3 obtained by fs-LA-MC-ICP-MS. The red line represents the literature value of MACS-3 of $^{87}Sr/^{86}Sr$ = 0.7075532 ± 0.0000037 (Jochum et al., 2011), the blue line shows the literature value of JCp-1 of $^{87}Sr/^{86}Sr$ =0.70916 ± 0.00002 (Ohno and Hirata, 2007), with its 2σ standard error shown as bright blue shading. The error range for the reference value of MACS-3 is too small to be visible in the figure. Note that sample MACS-3-8 was strongly affected by very variable ^{84}Kr intensities during the blank measurement and probably during the sample measurement as well.

5.3 Speleothem GP5

On sample GP5, a total number of 27 different layers were measured (Fig. 6 [A]). In the area between ~116 to 118.5 mm distance from top (DFT) the resolution is high (i.e. less than 100 µm between linescans). Further measurements were performed with a distance of ~1000 µm

between each other. Some measurements suffer from changing mass bias and low intensities ($^{88}Sr < 1$ V), resulting in decreasing values of $^{87}Sr/^{86}Sr$ (in particular linescans GP5-17-21, Table 2). The $^{87}Sr/^{86}Sr$ ratios generally show only minor variations, ranging from 0.70856 ± 0.00017 to 0.70920 ± 0.00007. The low-resolution measurements from 108.3 to 115.3 mm DFT show a relatively stable Sr isotope composition with $^{87}Sr/^{86}Sr$ ratios between 0.70890 ± 0.00011 and 0.70913 ± 0.00008. The average $^{87}Sr/^{86}Sr$ ratio of all linescans is 0.70892 ± 0.00006 (n = 79).

36 spot analyses were performed on stalagmite GP5. These were placed near the right end of the third linescan within the same growth layer (Fig. 1). At signal intensities lower than ca. 0.6 V on ^{88}Sr, we found a significant decrease of the $^{87}Sr/^{86}Sr$ ratio. Corresponding measurements are marked with double diamonds ♦♦ in Table 2. The $^{87}Sr/^{86}Sr$ ratios of the spot measurements from GP5 are presented as circles in Fig. 6 [A]. The results show a similar pattern as the linescans, even though the 2σ standard errors are slightly larger. The $^{87}Sr/^{86}Sr$ ratio varies between 0.70872 ± 0.00024 and 0.70907 ± 0.00011. The mean of all spot measurements is $^{87}Sr/^{86}Sr = 0.70897 \pm 0.00005$ (n = 32) and in good agreement with the linescan data.

5.4 Speleothem MAW-4

On MAW-4, 24 linescans were performed at a sampling resolution of 500 µm (Fig. 1). The $^{87}Sr/^{86}Sr$ ratios are presented in Fig. 6 [B]. While the first two measurements at 8.4 and 8.9 mm DFT are similar, the following measurements show a slightly increasing trend towards higher values, reaching a maximum of 0.70871 ± 0.00004. The 2σ standard error of all measurements is ± 0.00004 with an average $^{87}Sr/^{86}Sr$ ratio over all linescans of 0.70867 ± 0.00003 (n = 24).

24 spot analyses were performed on stalagmite MAW-4, placed near the right end of the third linescan within the same growth layer (Fig. 1). Note that layer MAW-4-7 was not measured.

For layer MAW-4-8, a total number of six spot measurements were performed to test the reproducibility. The mean of MAW-4-Spot-8a-c is within error of the mean of MAW-4-Spot-8d-f. Since MAW-4-Spot-8a-f are in perfect agreement, they were combined as a single measurement (MAW-4-Spot-8). The $^{87}Sr/^{86}Sr$ ratios of the spot measurements of MAW-4 are presented as circles in Fig. 6 [B]. A pattern, similar to the linescans can be observed with two measurements at 8.4 and 8.9 mm DFT showing lower $^{87}Sr/^{86}Sr$ ratios compared to the other values. In contrast to the linescan measurements, this increase is not significant due to larger errors. Nevertheless, an increase and a plateau at the same distance from top is visible for the spot analyses. The 2σ standard error of all measurements is in the range of ± 0.00006 to ± 0.00008 and therefore higher than for the linescans. The average $^{87}Sr/^{86}Sr$ ratio over all spot measurements is 0.70870 ± 0.00002 (n = 24), in agreement with the $^{87}Sr/^{86}Sr$ ratio derived from the linescans.

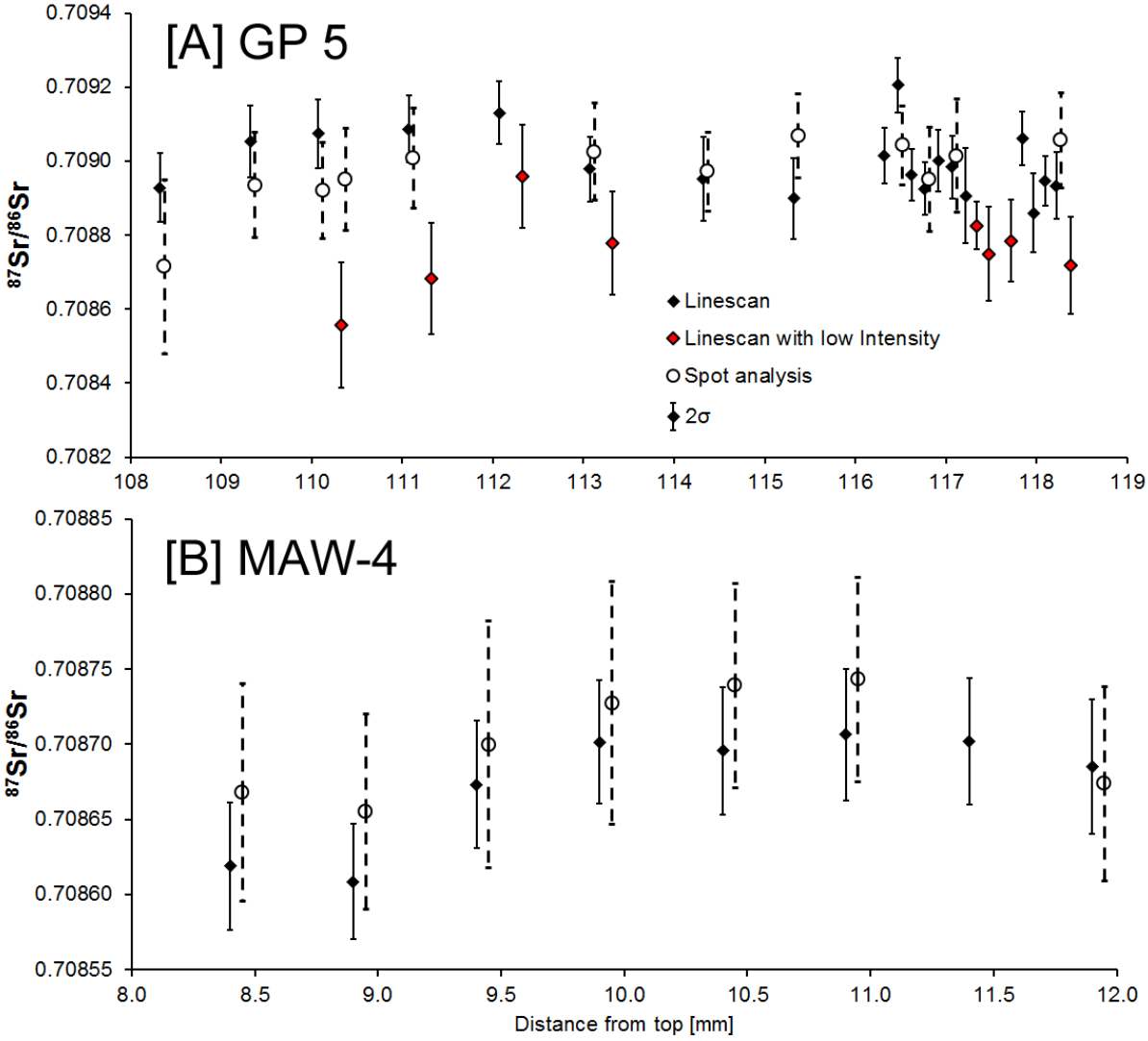

485

486 **Figure 6: [A]** $^{87}Sr/^{86}Sr$ ratios are plotted against the distance from top of speleothem GP5.
487 Linescan measurements affected by low signal intensities are marked red. **[B]** $^{87}Sr/^{86}Sr$ ratios
488 of speleothem MAW-4 against distance from top [mm] for the linescan as well as the spot
489 analyses. For better visualization of the error bars, spot analyses data were shifted to the right
490 by 0.05 mm.

491

492 **6. Discussion**

493 **6.1 Linescan versus spot analysis**

We used two different laser ablation methods for this study, i.e., linescans along growth bands and spots, to test which is the best approach. In general, the linescan method provides much smaller 2σ standard errors than the spot analysis. For RM JCt-1, the final $^{87}Sr/^{86}Sr$ ratio usually has a 2σ standard error in the range of ± 0.00002 – 0.00005 for linescan measurements, representing a total error in the range of 0.003 – 0.01 %. For spot analyses, the 2σ standard error was in the range of ± 0.00005 – 0.00007. The 2σ standard error is highly dependent on the Sr concentration of the sample (Fig. 7). The different precision in spot and linescan analyses is caused by: 1) the longer integration time for the linescan approach, and 2) decreasing signal intensity during spot analysis caused by deepening of the laser crater. Therefore, the spot analysis approach might be insufficiently precise to resolve small scale changes in the $^{87}Sr/^{86}Sr$ ratio. This is exemplified in MAW-4, where an increase in the $^{87}Sr/^{86}Sr$ ratio was significant for the linescan approach, but not for the spot analyses due to larger errors. A disadvantage of the linescan approach, however, is that unwanted sampling of material from different growth layers (with a different $^{87}Sr/^{86}Sr$ ratio) may occur. Furthermore, linescans require a larger sample surface compared to spot analysis. We recommend using the linescan approach only for speleothems with a regular (parallel) layering that provides a relatively large sample surface (ca. 3 mm width and length). For speleothems with irregular layering, spot analysis may be the preferable option. Tests with spot analyses showed that higher repetition rates (> 10 Hz) result in a higher signal intensity and precision, which is desirable for samples with relatively low Sr concentration (200-500 µg/g), such as GP5. However, the sample material should be dense and stable enough to resist such a high ablation efficiency. Higher repetition rates also result in deeper lased craters and thus potentially in ablating into different layers. However, for repetition rates in the range of 5 – 10 Hz the depth of the crater should be ≤12 µm and even less for linescan measurements (≤ 2 µm). Thus, this effect should only be important for very slowly growing speleothems.

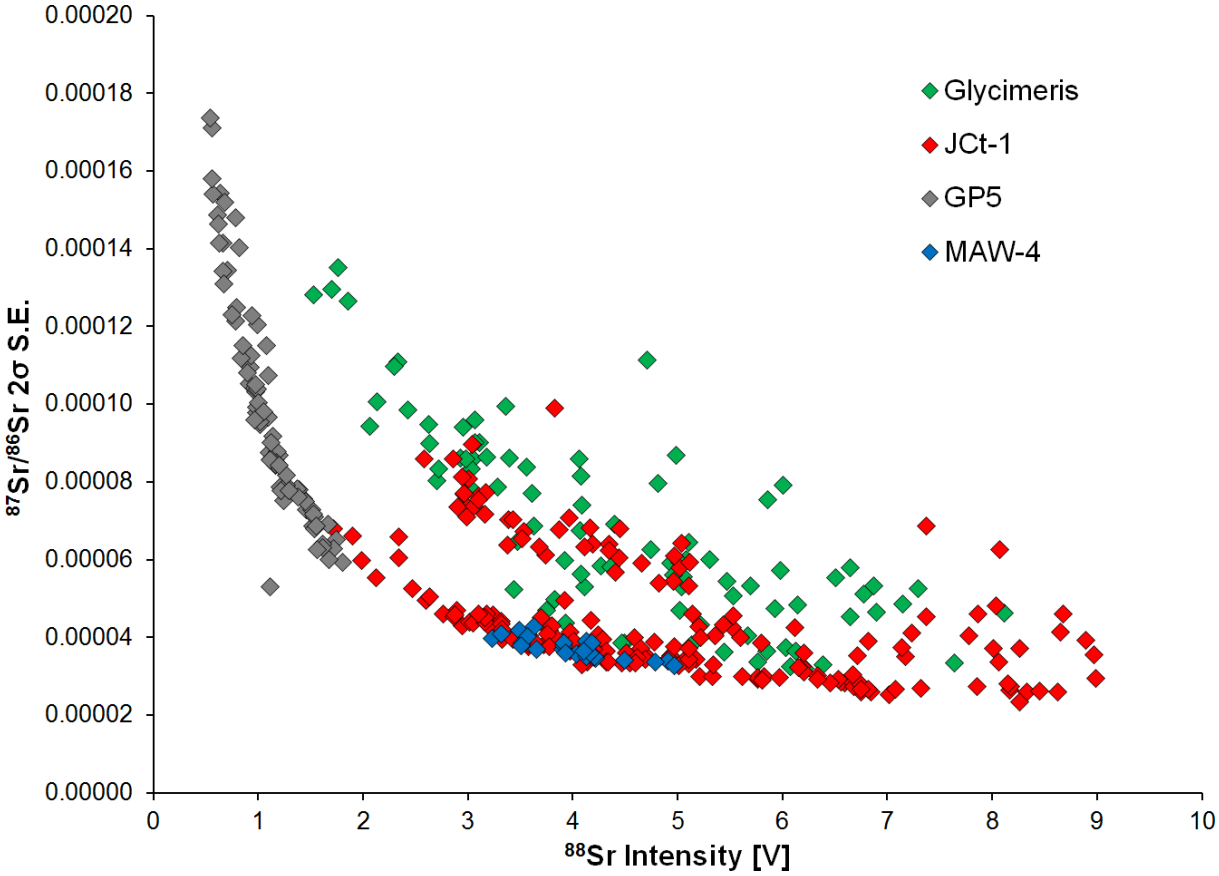

519

520 **Figure 7:** Scatter plot of ^{88}Sr intensity vs. $^{87}Sr/^{86}Sr$ 2σ standard error. The dependency of the
521 $^{87}Sr/^{86}Sr$ 2σ standard error on the ^{88}Sr intensity is shown for the linescan measurements of JCt-
522 1, *Glycimeris* sp., GP5 and MAW-4.

523

524 **6.2 Nanosecond versus femtosecond laser systems**

525 Ablating RMs JCp-1 and MACS-3 with either a nanosecond or a femtosecond laser gives
526 similar results. While the nanosecond laser provides the advantage of measuring lower
527 concentration samples with higher precision, the femtosecond laser is less vulnerable to
528 fractionation effects and offers better control on the ablation process (Glaus et al., 2010; Koch
529 and Gunther, 2007). In addition, the refractory Sr is generally less affected by matrix, elemental
530 and isotopic fractionation effects in comparison to the volatile Rb (Horn and von Blanckenburg,
531 2007). However, with our setup, the femtosecond laser approach requires much higher Sr

concentrations (> 1400 µg/g) to achieve sufficient precision. For instance, we were not able to accurately measure JCt-1 and our speleothem samples with the femtosecond laser due to insufficient Sr concentration. In contrast, the standard bracketing approach with JCt-1 and JCp-1 with the nanosecond laser was successful and the data from MACS-3 were similar to literature values. The results from the femtosecond LA-MC-ICP-MS measurements show that our approach can be transferred to other laser ablation systems. The raw measurements of JCp-1 and MACS-3 are in good agreement with literature values and the performance of our standard bracketing approach does not affect the resulting $^{87}Sr/^{86}Sr$ significantly. Overall, the $^{87}Sr/^{86}Sr$ RM data obtained with both laser ablation systems agree within error and are therefore probably not affected by differences in matrix effects between the different setups.

6.3. Tuning parameters and suitable reference materials

An aspect of major importance identified during the development of the LA-MC-ICP-MS technique is to adjust the tuning after changing the cones to obtain correct $^{87}Sr/^{86}Sr$ ratios of a reference solution. Tuning for maximum signal intensity does not always result in the $^{87}Sr/^{86}Sr$ ratio of the RM (Fig. 2). To achieve the correct $^{87}Sr/^{86}Sr$ ratio we adjusted the lens settings. In comparison to the tuning of the high voltage lenses, the source and transfer lenses had a larger effect on stability and reliability of the $^{87}Sr/^{86}Sr$ ratios with our NU Plasma MC-ICP-MS (Fig. 2). In addition, the laser ablation system itself alters the $^{87}Sr/^{86}Sr$ ratios of the measurements. Since different RMs and samples have variable Sr contents, the laser energy and spot size may have to be adjusted to prevent signal intensities larger than ~10 V on cup H4 (^{88}Sr signal). It is important to use similar measurement parameters for RMs and speleothem samples when the standard bracketing technique is applied. Therefore, it is essential to use a RM with similar Sr concentration and a similar matrix as the speleothem sample. By not using matrix-matched samples and RMs, potential differences in the occurrence of interference may alter the

557 correction (Irrgeher et al., 2016). In case of different matrices and/or large differences in Sr
558 concentration, the resulting $^{87}Sr/^{86}Sr$ ratio of the unknown sample needs to be handled with care
559 and might be less precise. For instance, the use of RM JCt-1 for correcting GP5 measurements
560 was critical, due to low intensities on the sample (1 – 2 V, ^{88}Sr) and high intensities on the RM
561 (up to 8 – 9 V, ^{88}Sr) when using the same laser parameters. Fluence decreases with laser energy
562 and it is not guaranteed that the same measurement parameters are available for all samples and
563 RMs. For speleothem samples with much higher Sr concentration than in this study, JCp-1 and
564 MACS-3 are suitable RMs.

565 Furthermore, the signal intensity of the Sr isotope measurements is important. Measurements
566 suffering from very low intensities on ^{88}Sr (~ < 1 V) show large errors. A scatter plot of the
567 intensity of the ^{88}Sr-signal against the 2σ standard error for the linescan measurements of JCt-
568 1, the bivalve shell of *Glycimeris* sp., GP5 and MAW-4 (Fig. 7) reveals in particular for GP5 a
569 high dependency on a sufficiently high Sr signal for precise measurements. Intensities of ^{88}Sr
570 below ~1.5 V cause a dramatic shift towards large errors. Similar patterns are visible for JCt-1
571 and the *Glycimeris* sp. shell. The Sr intensity difference found in MAW-4 is too low to show
572 the effect of signal intensity on the uncertainty. All measurements with low Sr intensities suffer
573 from low counting statistics and the background correction of Kr might be insufficient.

574 Another effect that can have major detrimental influence on the analysis is progressive clogging
575 of the cones. When a decrease in Sr intensity is observed, it is important to evaluate if this
576 change results from a change of the Sr content in the sample or from clogging of the cones by
577 deposition of Ca. Additional information on the performance of the mass spectrometer is
578 provided by monitoring the mass bias. In our study, the mass bias for the $^{87}Sr/^{86}Sr$-ratio was
579 usually between 0.45 – 2.09 % (R_{corr}/R_{meas} = 0.9791 – 0.9955, Eq. 3). Especially for the
580 linescans of sample MAW-4, the mass bias remained very stable (1.24 – 1.27 %; R_{corr}/R_{meas} =
581 0.9873 – 0.9877, Eq. 3). When the mass bias shows increased variability over the day, careful

582 evaluation of the results is necessary. We observed that a decrease in the $^{87}Sr/^{86}Sr$ ratio and an
583 increase in the 2σ standard error is often related to a high mass bias (e.g., for samples GP5-17-
584 21, Table 2).

585

586 **6.4 Standard bracketing**

587 Our results highlight the importance of the standard bracketing correction scheme for LA-MC-
588 ICP-MS Sr isotope analysis. Prior to the first sample measurements, a test of the standard
589 bracketing method was performed using JCt-1. For this purpose, JCt-1 was used as a RM and
590 also treated as a sample. The raw and corrected results are shown in Fig. 8. The standard
591 bracketing method seems to be generally applicable for $^{87}Sr/^{86}Sr$ ratio correction, since the
592 corrected Sr isotope ratios of JCt-1 agree within uncertainties. A similar test performed on the
593 RMs JCp-1 and MACS-3 with the femtosecond LA-MC-ICP-MS setup also showed reliable
594 results (Fig. 5).

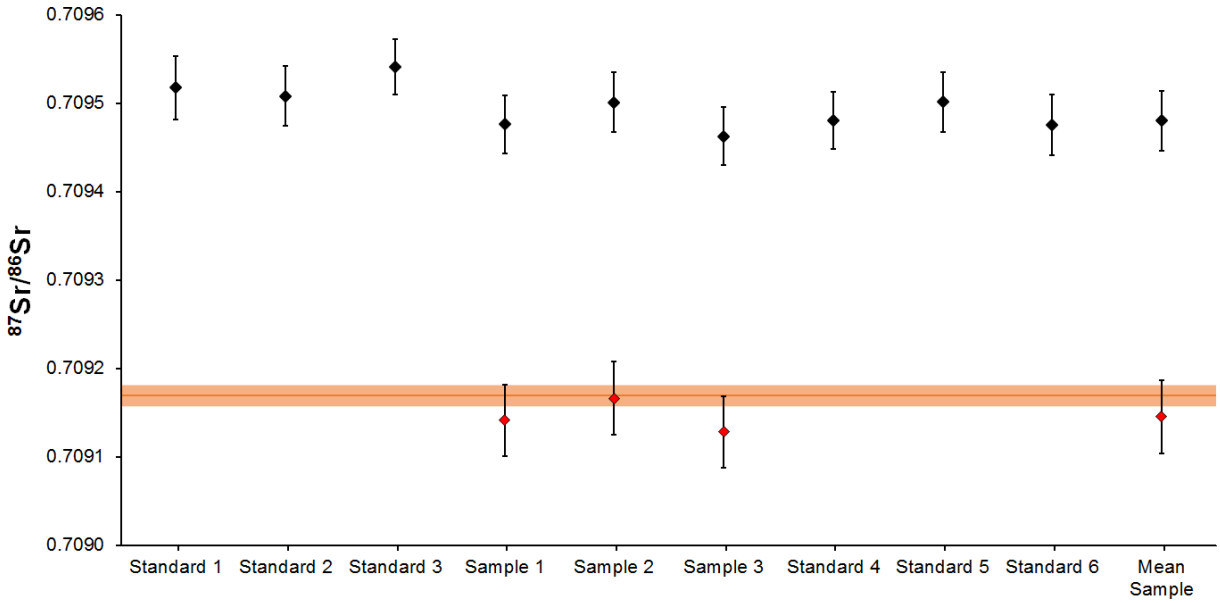

595

596 **Figure 8:** Black rhombs show the raw results of the $^{87}Sr/^{86}Sr$ LA-MC-ICP-MS linescan
597 measurements performed using JCt-1 as a reference material and a sample. Corrected $^{87}Sr/^{86}Sr$

598 ratios of JCt-1 are shown as red rhombs. Note that the errors increased in comparison to the raw
599 data due to correction via the reference material. The orange line represents the reference value
600 of JCt-1 of 0.70917 ± 0.00001 (Weber et al., In Revision).

601

602 **6.5 LA-MC-ICP-MS of Sr isotopes on speleothem samples**

603 Traditional Sr isotopes analysis by solution MC-ICP-MS or TIMS requires careful chemical
604 treatment. A recent study by Wortham et al. (2017) presented a speleothem Sr isotope record
605 obtained by LA-MC-ICP-MS. These authors performed linescan measurements parallel to the
606 growth axis of a speleothem from Brazil and traced an increasing $^{87}Sr/^{86}Sr$ ratio over the last
607 two millennia. Their approach is slightly different to ours. While their linescan is performed
608 parallel to the growth axis, we measure three linescans for each growth layer perpendicular to
609 the growth axis, which enables us to test whether results from individual growth layers are
610 reproducible (similar to the Hendy test for stable carbon and oxygen isotopes, Hendy (1971)).
611 In addition, the change of the $^{87}Sr/^{86}Sr$ ratio in the Brazilian speleothem was on the third
612 decimal, which is relatively large. Detecting smaller changes (i.e., on the fourth to fifth
613 decimal), is only possible by conducting a set of measurements perpendicular to the growth
614 axis. Otherwise the obtained $^{87}Sr/^{86}Sr$ ratio is largely influenced by a time-averaging effect.
615 Wortham et al. (2017) used a different sampling approach and do not provide the Sr
616 concentration of their speleothem and the used RM which complicates the comparison of both
617 studies. Nevertheless, they showed that it is possible to track large changes in speleothem Sr
618 isotope ratios using linescans parallel to the growth axis. Our results show that it is also possible
619 to obtain higher precision Sr isotope data by LA-MC-ICP-MS using a set of linescans, as well
620 as spot analyses orientated perpendicular to the growth axis. With the state-of-the-art MC-ICP-
621 MS systems, it is unlikely that small scale changes in Sr isotope composition can be detected
622 by performing a linescan parallel to the growth axis. This is further complicated by the typically

low Sr concentration of speleothems (few hundred µg/g or even less). However, aragonitic speleothems can have much higher Sr concentrations of several thousand µg/g. Thus, in aragonitic samples, a linescan parallel to the growth axis may reveal small-scale changes in Sr isotope composition.

7. Conclusions

We show that LA-MC-ICP-MS is a powerful tool for the analysis of Sr isotopes in speleothems. Best results are obtained from samples with Sr concentrations of >1000 µg/g. For our setup, the minimum ^{88}Sr concentration required to obtain reliable $^{87}Sr/^{86}Sr$ ratios was ca. 300 µg/g. In order to retrieve reliable results, appropriate tuning of both the mass spectrometer and the laser ablation system is of great importance. Tuning for maximum intensity does not always result in correct $^{87}Sr/^{86}Sr$ ratios. We highly recommend to tune for the correct Sr-isotope ratio of a reference material prior to an analytical session. The Sr concentration of the RM should be in the same range as that in the samples. In order to account for potential drifts in the mass spectrometer during an analytical session, we recommend to apply standard bracketing using appropriate RMs.

Linescans provide higher precision than spot analyses. The latter might be advantageous however if only a limited surface is available for sampling, for instance in case of a irregular layering. While speleothem samples tested here contain only low amounts of REEs and Rb, appropriate correction procedures are required to minimise the influence of interferences from these elements. In addition, potential interferences resulting from Ca argides and dimers should be accounted for.

The use of a femtosecond laser ablation system provides a more stable signal intensity and therefore more precise measurements, but its application on samples with low Sr concentrations

(ca. >1400 µg/g, since measurements with JCt-1 were not precise enough) is not recommended due to lower signal intensities compared to the nanosecond laser leading to less precise results.

Acknowledgements

M. Weber, J.A. Wassenburg, K.P. Jochum and D. Scholz are thankful to the Max Planck Graduate Center and the German Research Foundation (DFG WA3532-1/1 and DFG SCHO 1274/9-1) for funding. S. Breitenbach and D. Scholz acknowledge financial support from the European Union's Horizon 2020 Research and Innovation program under the Marie Skłodowska-Curie grant agreement No 691037 (QUEST). We also thank B. Schwager, B. Stoll, U. Weis, C. Obert, A. Budsky and F. Lugli for assistance in the laboratory. The authors thank the editor Klaus Mezger, Alison Koleszar and one anonymous referee for their thorough reviews and constructive comments, which helped to improve the manuscript.

References

Aizawa, S., 2008. Determination of trace elements in carbonate reference samples by instrumental neutron activation analysis. Journal of Radioanalytical and Nuclear Chemistry, 278(2): 349-352.

Asmerom, Y., Polyak, V.J., Burns, S.J., 2010. Variable winter moisture in the southwestern United States linked to rapid glacial climate shifts. Nature Geoscience, 3(2): 114-117.

Avigour, A., Magaritz, M., Issar, A., Dodson, M.H., 1990. Sr Isotope Study of Vein and Cave Calcites from Southern Israel. Chemical Geology, 82(1-2): 69-81.

Ayalon, A., Bar-Matthews, M., Kaufman, A., 1999. Petrography, strontium, barium and uranium concentrations, and strontium and uranium isotope ratios in speleothems as palaeoclimatic proxies: Soreq Cave, Israel. Holocene, 9(6): 715-722.

Banner, J.L., 2004. Radiogenic isotopes: systematics and applications to earth surface processes and chemical stratigraphy. Earth-Science Reviews, 65(3-4): 141-194.

Banner, J.L., Kaufman, J., 1994. The isotopic record of ocean chemistry and diagenesis preserved in non-luminescent brachiopods from Mississippian carbonate rocks, Illinois and Missouri. Geological Society of America Bulletin, 106(8): 1074-1082.

Banner, J.L., Musgrove, M., Capo, R.C., 1994. Tracing ground-water evolution in a limestone aquifer using Sr isotopes: Effects of multiple sources of dissolved ions and mineral-solution reactions. Geology, 22(8): 687-690.

Banner, J.L., Musgrove, M.L., Asmerom, Y., Edwards, R.L., Hoff, J.A., 1996. High-resolution temporal record of Holocene ground-water chemistry: Tracing links between climate and hydrology. Geology, 24(11): 1049-1053.

Bar-Matthews, M., Ayalon, A., Kaufman, A., Wasserburg, G.J., 1999. The Eastern Mediterranean paleoclimate as a reflection of regional events: Soreq cave, Israel. Earth and Planetary Science Letters, 166(1-2): 85-95.

Barnett-Johnson, R., Ramos, F.C., Grimes, C.B., MacFarlane, R.B., 2005. Validation of Sr isotopes in otoliths by laser ablation multicollector inductively coupled plasma mass spectrometry (LA-MC-ICPMS): opening avenues in fisheries science applications. Canadian Journal of Fisheries and Aquatic Sciences, 62(11): 2425-2430.

Berglund, M., Wieser, M.E., 2011. Isotopic compositions of the elements 2009 (IUPAC Technical Report). Pure and Applied Chemistry, 83(2): 397-410.

Bizzarro, M., Simonetti, A., Stevenson, R.K., Kurszlaukis, S., 2003. In situ 87Sr/86Sr investigation of igneous apatites and carbonates using laser-ablation MC-ICP-MS. Geochimica et Cosmochimica Acta, 67(2): 289-302.

Breitenbach, S.F.M., Adkins, J.F., Meyer, H., Marwan, N., Kumar, K.K., Haug, G.H., 2010. Strong influence of water vapor source dynamics on stable isotopes in precipitation observed in Southern Meghalaya, NE India. Earth and Planetary Science Letters, 292(1-2): 212-220.

Breitenbach, S.F.M., Lechleitner, F.A., Meyer, H., Diengdoh, G., Mattey, D., Marwan, N., 2015. Cave ventilation and rainfall signals in dripwater in a monsoonal setting - a monitoring study from NE India. Chemical Geology, 402: 111-124.

Cheng, H., Edwards, R.L., Sinha, A., Spötl, C., Yi, L., Chen, S., Kelly, M., Kathayat, G., Wang, X., Li, X., 2016. The Asian monsoon over the past 640,000 years and ice age terminations. Nature, 534(7609): 640-646.

Christensen, J.N., Halliday, A.N., Lee, D.C., Hall, C.M., 1995. In-Situ Sr Isotopic Analysis by Laser-Ablation. Earth and Planetary Science Letters, 136(1-2): 79-85.

Copeland, S.R., Sponheimer, M., le Roux, P.J., Grimes, V., Lee-Thorp, J.A., de Ruiter, D.J., Richards, M.P., 2008. Strontium isotope ratios (87Sr/86Sr) of tooth enamel: a comparison of solution and laser ablation multicollector inductively coupled plasma mass spectrometry methods. Rapid Commun Mass Spectrom, 22(20): 3187-94.

Copeland, S.R., Sponheimer, M., Lee-Thorp, J.A., le Roux, P.J., de Ruiter, D.J., Richards, M.P., 2010. Strontium isotope ratios in fossil teeth from South Africa: assessing laser ablation MC-ICP-MS analysis and the extent of diagenesis. Journal of Archaeological Science, 37(7): 1437-1446.

709 Cruz, F.W., Burns, S.J., Karmann, I., Sharp, W.D., Vuille, M., Cardoso, A.O., Ferrari, J.A., Dias, P.L.S.,
710 Viana, O., 2005. Insolation-driven changes in atmospheric circulation over the past 116,000
711 years in subtropical Brazil. Nature, 434(7029): 63-66.
712 Davidson, J., Tepley, F., Palacz, Z., Meffan-Main, S., 2001. Magma recharge, contamination and
713 residence times revealed by in situ laser ablation isotopic analysis of feldspar in volcanic rocks.
714 Earth and Planetary Science Letters, 184(2): 427-442.
715 Ehrlich, S., Gavrieli, I., Dor, L.-B., Halicz, L., 2001. Direct high-precision measurements of the 87Sr/86Sr
716 isotope ratio in natural water, carbonates and related materials by multiple collector
717 inductively coupled plasma mass spectrometry (MC-ICP-MS). Journal of Analytical Atomic
718 Spectrometry, 16(12): 1389-1392.
719 Fairchild, I.J., Borsato, A., Tooth, A.F., Frisia, S., Hawkesworth, C.J., Huang, Y., McDermott, F., Spiro, B.,
720 2000. Controls on trace element (Sr–Mg) compositions of carbonate cave waters: implications
721 for speleothem climatic records. Chemical Geology, 166(3–4): 255-269.
722 Fairchild, I.J., Smith, C.L., Baker, A., Fuller, L., Spotl, C., Mattey, D., McDermott, F., Eimp, 2006.
723 Modification and preservation of environmental signals in speleothems. Earth-Science
724 Reviews, 75(1-4): 105-153.
725 Fairchild, I.J., Treble, P.C., 2009. Trace elements in speleothems as recorders of environmental change.
726 Quaternary Science Reviews, 28(5-6): 449-468.
727 Faure, G., Mensing, T.M., 2005. Isotopes: principles and applications. Wiley, 897 pp.
728 Fisher, E.C., Bar-Matthews, M., Jerardino, A., Marean, C.W., 2010. Middle and Late Pleistocene
729 paleoscape modeling along the southern coast of South Africa. Quaternary Science Reviews,
730 29(11-12): 1382-1398.
731 Frumkin, A., Stein, M., 2004. The Sahara-East Mediterranean dust and climate connection revealed by
732 strontium and uranium isotopes in a Jerusalem speleothem. Earth and Planetary Science
733 Letters, 217(3-4): 451-464.
734 Genty, D., Blamart, D., Ouahdi, R., Gilmour, M., Baker, A., Jouzel, J., Van-Exter, S., 2003. Precise dating
735 of Dansgaard-Oeschger climate oscillations in western Europe from stalagmite data. Nature,
736 421(6925): 833-837.
737 Glaus, R., Kaegi, R., Krumeich, F., Gunther, D., 2010. Phenomenological studies on structure and
738 elemental composition of nanosecond and femtosecond laser-generated aerosols with
739 implications on laser ablation inductively coupled plasma mass spectrometry. Spectrochimica
740 Acta Part B-Atomic Spectroscopy, 65(9-10): 812-822.
741 Goede, A., McCulloch, M., McDermott, F., Hawkesworth, C., 1998. Aeolian contribution to strontium
742 and strontium isotope variations in a Tasmanian speleothem. Chemical Geology, 149(1-2): 37-
743 50.
744 Hendy, C.H., 1971. The isotopic geochemistry of speleothems—I. The calculation of the effects of
745 different modes of formation on the isotopic composition of speleothems and their
746 applicability as palaeoclimatic indicators. Geochimica et Cosmochimica Acta, 35(8): 801-824.
747 Hoffmann, D.L., Rogerson, M., Spötl, C., Luetscher, M., Vance, D., Osborne, A.H., Fello, N.M., Moseley,
748 G.E., 2016. Timing and causes of North African wet phases during the last glacial period and
749 implications for modern human migration. Scientific reports, 6.
750 Hori, M., Ishikawa, T., Nagaishi, K., Lin, K., Wang, B.-S., You, C.-F., Shen, C.-C., Kano, A., 2013. Prior
751 calcite precipitation and source mixing process influence Sr/Ca, Ba/Ca and 87Sr/86Sr of a
752 stalagmite developed in southwestern Japan during 18.0–4.5ka. Chemical Geology, 347: 190-
753 198.
754 Horn, I., von Blanckenburg, F., 2007. Investigation on elemental and isotopic fractionation during 196
755 nm femtosecond laser ablation multiple collector inductively coupled plasma mass
756 spectrometry. Spectrochimica Acta Part B-Atomic Spectroscopy, 62(4): 410-422.
757 Ingle, C.P., Sharp, B.L., Horstwood, M.S.A., Parrish, R.R., Lewis, D.J., 2003. Instrument response
758 functions, mass bias and matrix effects in isotope ratio measurements and semi-quantitative
759 analysis by single and multi-collector ICP-MS. Journal of Analytical Atomic Spectrometry, 18(3):
760 219-229.

761 Irrgeher, J., Galler, P., Prohaska, T., 2016. 87 Sr/86 Sr isotope ratio measurements by laser ablation
762 multicollector inductively coupled plasma mass spectrometry: Reconsidering matrix
763 interferences in bioapatites and biogenic carbonates. Spectrochimica Acta Part B: Atomic
764 Spectroscopy, 125: 31-42.
765 Jackson, M.G., Hart, S.R., 2006. Strontium isotopes in melt inclusions from Samoan basalts:
766 Implications for heterogeneity in the Samoan plume. Earth and Planetary Science Letters,
767 245(1-2): 260-277.
768 Jochum, K.P., Nohl, L., Herwig, K., Lammel, E., Stoll, B., Hofmann, A.W., 2005. GeoReM: A new
769 geochemical database for reference materials and isotopic standards. Geostandards and
770 Geoanalytical Research, 29(3): 333-338.
771 Jochum, K.P., Scholz, D., Stoll, B., Weis, U., Wilson, S.A., Yang, Q.C., Schwalb, A., Borner, N., Jacob, D.E.,
772 Andreae, M.O., 2012. Accurate trace element analysis of speleothems and biogenic calcium
773 carbonates by LA-ICP-MS. Chemical Geology, 318: 31-44.
774 Jochum, K.P., Stoll, B., Weis, U., Kuzmin, D.V., Sobolev, A.V., 2009. In situ Sr isotopic analysis of low Sr
775 silicates using LA-ICP-MS. Journal of Analytical Atomic Spectrometry, 24(9): 1237-1243.
776 Jochum, K.P., Wilson, S.A., Abouchami, W., Amini, M., Chmeleff, J., Eisenhauer, A., Hegner, E., Iaccheri,
777 L.M., Kieffer, B., Krause, J., McDonough, W.F., Mertz-Kraus, R., Raczek, I., Rudnick, R.L., Scholz,
778 D., Steinhoefel, G., Stoll, B., Stracke, A., Tonarini, S., Weis, D., Weis, U., Woodhead, J.D., 2011.
779 GSD-1G and MPI-DING Reference Glasses for In Situ and Bulk Isotopic Determination.
780 Geostandards and Geoanalytical Research, 35(2): 193-226.
781 Kennett, D.J., Breitenbach, S.F.M., Aquino, V.V., Asmerom, Y., Awe, J., Baldini, J.U.L., Bartlein, P.,
782 Culleton, B.J., Ebert, C., Jazwa, C., 2012. Development and disintegration of Maya political
783 systems in response to climate change. Science, 338(6108): 788-791.
784 Koch, J., Gunther, D., 2007. Femtosecond laser ablation inductively coupled plasma mass
785 spectrometry: achievements and remaining problems. Anal Bioanal Chem, 387(1): 149-53.
786 Li, H.-C., Ku, T.-L., You, C.-F., Cheng, H., Edwards, R.L., Ma, Z.-B., Tsai, W.-s., Li, M.-D., 2005. 87Sr/86Sr
787 and Sr/Ca in speleothems for paleoclimate reconstruction in Central China between 70 and
788 280 kyr ago. Geochimica et Cosmochimica Acta, 69(16): 3933-3947.
789 Luetscher, M., Boch, R., Sodemann, H., Spotl, C., Cheng, H., Edwards, R.L., Frisia, S., Hof, F., Muller, W.,
790 2015. North Atlantic storm track changes during the Last Glacial Maximum recorded by Alpine
791 speleothems. Nat Commun, 6: 6344.
792 McDermott, F., 2004. Palaeo-climate reconstruction from stable isotope variations in speleothems: a
793 review. Quaternary Science Reviews, 23(7-8): 901-918.
794 Müller, W., Anczkiewicz, R., 2016. Accuracy of laser-ablation (LA)-MC-ICPMS Sr isotope analysis of (bio)
795 apatite–a problem reassessed. Journal of Analytical Atomic Spectrometry, 31(1): 259-269.
796 Ohno, T., Hirata, T., 2007. Simultaneous determination of mass-dependent isotopic fractionation and
797 radiogenic isotope variation of strontium in geochemical samples by multiple collector-ICP-
798 mass spectrometry. Anal Sci, 23(11): 1275-80.
799 Oster, J.L., Montañez, I.P., Guilderson, T.P., Sharp, W.D., Banner, J.L., 2010. Modeling speleothem δ13C
800 variability in a central Sierra Nevada cave using 14C and 87Sr/86Sr. Geochimica et
801 Cosmochimica Acta, 74(18): 5228-5242.
802 Oster, J.L., Montañez, I.P., Mertz-Kraus, R., Sharp, W.D., Stock, G.M., Spero, H.J., Tinsley, J., Zachos,
803 J.C., 2014. Millennial-scale variations in western Sierra Nevada precipitation during the last
804 glacial cycle MIS 4/3 transition. Quaternary Research, 82(1): 236-248.
805 Outridge, P., Chenery, S., Babaluk, J., Reist, J., 2002. Analysis of geological Sr isotope markers in fish
806 otoliths with subannual resolution using laser ablation-multicollector-ICP-mass spectrometry.
807 Environmental Geology, 42(8): 891-899.
808 Poitrasson, F., Mao, X., Mao, S.S., Freydier, R., Russo, R.E., 2003. Comparison of ultraviolet
809 femtosecond and nanosecond laser ablation inductively coupled plasma mass spectrometry
810 analysis in glass, monazite, and zircon. Anal Chem, 75(22): 6184-90.
811 Ramos, F.C., Wolff, J.A., Tollstrup, D.L., 2004. Measuring 87Sr/86Sr variations in minerals and
812 groundmass from basalts using LA-MC-ICPMS. Chemical Geology, 211(1–2): 135-158.

Richards, D.A., Dorale, J.A., 2003. Uranium-series Chronology and Environmental Applications of Speleothems. Reviews in Mineralogy and Geochemistry, 52(1): 407.
Scholz, D., Hoffmann, D., 2008. 230Th/U-dating of fossil corals and speleothems. Quaternary Science Journal, 57(1–2): 52–76.
Steiger, R.H., Jäger, E., 1977. Subcommission on geochronology: Convention on the use of decay constants in geo- and cosmochronology. Earth and Planetary Science Letters, 36(3): 359-362.
Vanhaecke, F., Resano, M., Koch, J., McIntosh, K., Günther, D., 2010. Femtosecond laser ablation-ICP-mass spectrometry analysis of a heavy metallic matrix: Determination of platinum group metals and gold in lead fire-assay buttons as a case study. Journal of Analytical Atomic Spectrometry, 25(8): 1259.
Verheyden, S., Keppens, E., Fairchild, I.J., McDermott, F., Weis, D., 2000. Mg, Sr and Sr isotope geochemistry of a Belgian Holocene speleothem: implications for paleoclimate reconstructions. Chemical Geology, 169(1-2): 131-144.
Waight, T., Baker, J., Peate, D., 2002. Sr isotope ratio measurements by double-focusing MC-ICPMS: techniques, observations and pitfalls. International Journal of Mass Spectrometry, 221(3): 229-244.
Wang, Y.-J., Cheng, H., Edwards, R.L., An, Z.S., Wu, J.Y., Shen, C.C., Dorale, J.A., 2001. A high-resolution absolute-dated late Pleistocene monsoon record from Hulu Cave, China. Science, 294(5550): 2345-2348.

Wassenburg, J.A., Immenhauser, A., Richter, D.K., Jochum, K.P., Fietzke, J., Deininger, M., Goos, M., Scholz, D., Sabaoui, A., 2012. Climate and cave control on Pleistocene/Holocene calcite-to-aragonite transitions in speleothems from Morocco: Elemental and isotopic evidence. Geochimica et Cosmochimica Acta, 92: 23-47.
Wassenburg, J.A., Immenhauser, A., Richter, D.K., Niedermayr, A., Riechelmann, S., Fietzke, J., Scholz, D., Jochum, K.P., Fohlmeister, J., Schröder-Ritzrau, A., Sabaoui, A., Riechelmann, D.F.C., Schneider, L., Esper, J., 2013. Moroccan speleothem and tree ring records suggest a variable positive state of the North Atlantic Oscillation during the Medieval Warm Period. Earth and Planetary Science Letters, 375: 291-302.
Wassenburg, J.A., Dietrich, S., Fietzke, J., Fohlmeister, J., Jochum, K.P., Scholz, D., Richter, D.K., Sabaoui, A., Spotl, C., Lohmann, G., Andreae, M.O., Immenhauser, A., 2016a. Reorganization of the North Atlantic Oscillation during early Holocene deglaciation. Nature Geoscience, 9(8): 602-605.
Wassenburg, J.A., Scholz, D., Jochum, K.P., Cheng, H., Oster, J., Immenhauser, A., Richter, D.K., Hager, T., Jamieson, R.A., Baldini, J.U.L., Hoffmann, D., Breitenbach, S.F.M., 2016b. Determination of aragonite trace element distribution coefficients from speleothem calcite-aragonite transitions. Geochimica et Cosmochimica Acta, 190: 347-367.
Weber, M., Lugli, F., Jochum, K.P., Cipriani, A., Scholz, D., In Revision. Calcium carbonate and phosphate reference materials for monitoring bulk and micoranalytical analysis of Sr isotopes. Geostandards and Geoanalytical Research.
Woodhead, J., Swearer, S., Hergt, J., Maas, R., 2005. In situ Sr-isotope analysis of carbonates by LA-MC-ICP-MS: interference corrections, high spatial resolution and an example from otolith studies. Journal of Analytical Atomic Spectrometry, 20(1): 22.
Wortham, B.E., Wong, C.I., Silva, L.C.R., McGee, D., Montañez, I.P., Rasbury, E.T., Cooper, K.M., Sharp, W.D., Glessner, J.J.G., Santos, R.V., 2017. Assessing response of local moisture conditions in central Brazil to variability in regional monsoon intensity using speleothem 87Sr/86Sr values. Earth and Planetary Science Letters.
Zhou, H., Feng, Y.-x., Zhao, J.-x., Shen, C.-C., You, C.-F., Lin, Y., 2009. Deglacial variations of Sr and 87Sr/86Sr ratio recorded by a stalagmite from Central China and their association with past climate and environment. Chemical Geology, 268(3–4): 233-247.

Table 1: NU Plasma collector block assignments used for *in-situ* LA-MC-ICP-MS Sr isotope analysis of speleothems. Collectors H1, H2, H4, Ax and L1 – L5 are Faraday cups, IC-1 is an ion counter.

Collector	**H4**	**H2**	**H1**	**Ax**	**L1**	**L2**	**L3**	**IC-1**	**L4**	**L5**
Single Mass	88	87	86.5	86	85.5	85	84	83.5	83	82
Double Mass	176	174	173	172	171	170	168	167	166	164
Isotope of interest	$^{88}Sr_{82.58\%}$	$^{87}Sr_{7.00\%}$	-	$^{86}Sr_{9.86\%}$	-	-	$^{84}Sr_{0.56\%}$	-	-	-
Singly-charged interferences	-	$^{87}Rb_{27.83\%}$	-	$^{86}Kr_{17.28\%}$	-	$^{85}Rb_{72.17\%}$	$^{84}Kr_{56.99\%}$	-	$^{83}Kr_{11.50\%}$	$^{82}Kr_{11.59\%}$
Doubly-charged	$^{176}Yb_{12.99\%}$	$^{174}Yb_{32.03\%}$	$^{173}Yb_{16.10\%}$	$^{172}Yb_{21.68\%}$	$^{171}Yb_{14.09\%}$	$^{170}Yb_{2.98\%}$	$^{168}Yb_{0.12\%}$	-	-	-
interferences	-	-	-	-	-	$^{170}Er_{14.91\%}$	$^{168}Er_{26.98\%}$	$^{167}Er_{22.87\%}$	$^{166}Er_{33.50\%}$	$^{164}Er_{1.60\%}$
Molecular	$^{40}Ca^{48}Ca$	$^{44}Ca^{43}Ca$	-	$^{40}Ca^{46}Ca$	-	$^{42}Ca^{43}Ca$	$^{40}Ca^{44}Ca$	-	$^{40}Ca^{43}Ca$	$^{40}Ca^{42}Ca$
interferences	$^{40}Ar^{48}Ca$	-	-	$^{40}Ar^{46}Ca$	-	-	$^{40}Ar^{44}Ca$	-	$^{40}Ar^{43}Ca$	$^{40}Ar^{42}Ca$

Note that only collectors used during analysis are shown in this table. Potential interferences affecting the Sr masses are also illustrated along with natural abundances for Sr, Rb, Kr, Yb and Er (Berglund and Wieser (2011). Abundances for molecular interferences of Ca dimers and argides are not

871 shown for reasons of clarity. Some masses have a large number of potential interferences of Ca argides and dimers (e.g. mass 86 with $^{43}Ca^{43}Ca$,
872 $^{40}Ca^{46}Ca$, $^{42}Ca^{44}Ca$, $^{48}Ca^{38}Ar$, $^{46}Ca^{40}Ar$). Here, only the two most common molecular interferences are shown. Prior to each analysis, the peak center
873 was determined on mass 84 (L3) using the signal of ^{84}Kr in the gas flow of Ar. Therefore, mass 84 is underlined.

874 **Table 2:** Results of the linescan analysis from speleothem samples GP5 and MAW-4. The
875 alignment of the different cups is presented with the corresponding signal intensities. For most
876 sample layers, three runs were performed. For these samples, the mean of all runs is shown.

877

878 ♦ Sr-concentrations for sample GP5 were taken from Wassenburg et al. (2013) and Sr-
879 concentrations for sample MAW-4 were taken from Wassenburg et al. (2016b).

880 ♦♦ Not all of the three measurements from each spot were taken into account due to shifts in
881 the $^{87}Sr/^{86}Sr$ ratio of measurements with low Sr-intensities (approximately below 0.7 V for
882 ^{88}Sr).

Sample	Distance from top [mm]	x̄ ♦Sr conc [µg/g]	x̄ Total Sr [V]	x̄ Total Rb [mV]	x̄ Rb/Sr *10^{-3}	x̄ Er/Sr *10^{-6}	x̄ Yb/Sr *10^{-6}	x̄ $^{87}Sr/^{86}Sr$	x̄ 2σ Std Err	x̄ Mass Bias $^{87}Sr/^{86}Sr$	Sample	Distance from top [mm]	x̄ Total Sr [V]	x̄ Total Rb [mV]	x̄ Rb/Sr *10^{-3}	x̄ Er/Sr *10^{-6}	x̄ Yb/Sr *10^{-6}	x̄ $^{87}Sr/^{86}Sr$	x̄ 2σ Std Err	x̄ Mass Bias $^{87}Sr/^{86}Sr$
Linescans GP5											*Spotscans*									
GP5-1	118.4	344	0.9	0.08	0.09	1.3	703	0.70872	0.00013	1.23%										
GP5-2	118.2	349	1.4	0.08	0.06	1.3	257	0.70893	0.00009	1.22%	GP5-Spot-2	118.2	1.4	0.12	0.08	3.4	529	0.70906	0.00013	1.18%
GP5-3	118.0	354	1.2	0.12	0.10	1.0	419	0.70886	0.00011	1.22%										
GP5-4	117.7	310	1.1	0.08	0.07	1.0	~ 0	0.70879	0.00011	1.21%										
GP5-5	117.5	292	1.2	0.10	0.09	1.0	1136	0.70875	0.00013	1.20%										
GP5-6	117.2	354	1.1	0.10	0.09	1.1	664	0.70891	0.00013	1.20%										
GP5-7	117.3	328	1.3	0.06	0.04	1.3	~ 0	0.70883	0.00006	1.18%										
GP5-8	118.1	357	2.1	0.12	0.05	1.2	363	0.70895	0.00007	1.02%										
GP5-9	117.8	335	2.0	0.13	0.06	1.2	497	0.70906	0.00007	1.05%										
GP5-10	117.1	343	1.5	0.19	0.13	1.0	121	0.70898	0.00009	1.14%	GP5-Spot-10	117.1	1.0	0.10	0.09	3.5	865	0.70901	0.00015	1.12%
GP5-11	116.9	321	1.6	0.12	0.07	0.9	424	0.70900	0.00008	1.31%										
GP5-12	116.8	348	1.9	0.16	0.08	1.0	349	0.70893	0.00007	1.05%	GP5-Spot-12	116.8	1.4	0.11	0.08	2.7	919	0.70895	0.00014	1.95%
GP5-13	116.6	338	1.9	0.15	0.08	1.1	289	0.70896	0.00007	1.07%										
GP5-14	116.5	340	1.8	0.11	0.06	1.0	268	0.70920	0.00007	1.38%	GP5-Spot-14	116.5	1.7	0.13	0.08	2.7	327	0.70904	0.00011	1.92%
GP5-15	116.3	336	1.8	0.13	0.07	1.0	803	0.70902	0.00008	1.61%										
GP5-16	115.3	385	1.2	0.20	0.17	1.0	405	0.70890	0.00011	1.75%	GP5-Spot-16	115.3	1.6	0.08	0.05	2.7	487	0.70907	0.00011	1.93%
GP5-17	114.3	416	1.1	0.10	0.10	1.0	501	0.70895	0.00011	2.03%	GP5-Spot-17♦♦	114.3	1.1	0.08	0.08	2.6	1116	0.70897	0.00011	1.87%
GP5-18	113.3	353	0.9	0.14	0.16	1.1	441	0.70878	0.00014	2.09%										
GP5-19	112.3	363	0.8	0.17	0.22	1.1	179	0.70896	0.00014	1.82%										
GP5-20	111.3	381	0.7	0.16	0.22	0.9	136	0.70868	0.00015	1.87%										
GP5-21	110.3	427	0.7	0.13	0.19	1.1	285	0.70856	0.00017	2.23%	GP5-Spot-21	110.3	1.1	0.08	0.07	3.5	867	0.70895	0.00014	1.94%
GP5-22	113.1	351	1.4	0.26	0.18	1.4	435	0.70898	0.00009	1.19%	GP5-Spot-22	113.1	1.2	0.07	0.06	2.9	757	0.70903	0.00013	1.91%
GP5-23	112.1	425	1.5	0.19	0.13	1.6	~ 0	0.70913	0.00008	1.18%										
GP5-24	111.1	384	1.4	0.16	0.12	1.6	91	0.70909	0.00009	1.16%	GP5-Spot-24♦♦	111.1	0.9	0.11	0.12	3.0	763	0.70901	0.00014	1.93%
GP5-25	110.1	497	1.3	0.16	0.12	1.5	~ 0	0.70907	0.00009	1.16%	GP5-Spot-25	110.1	1.3	0.08	0.06	2.9	244	0.70892	0.00013	1.96%
GP5-26	109.3	412	1.3	0.20	0.16	1.7	~ 0	0.70905	0.00010	1.16%	GP5-Spot-26♦♦	109.3	1.1	0.12	0.12	3.3	564	0.70894	0.00014	1.98%
GP5-27	108.3	373	1.4	0.23	0.17	1.6	233	0.70893	0.00009	1.16%	GP5-Spot-27♦♦	108.3	0.5	0.06	0.12	2.8	708	0.70872	0.00024	2.00%
Linescans MAW4											*Spotscans*									
MAW4-1	8.4	1729	4.8	0.06	0.01	0.4	1181	0.70862	0.00004	1.24%	MAW4-Spot-1	8.4	4.1	0.15	0.04	1.3	432	0.70867	0.00007	0.92%
MAW4-2	8.9	1629	5.7	0.03	0.01	0.4	2295	0.70861	0.00004	1.25%	MAW4-Spot-2	8.9	3.6	0.08	0.02	1.2	694	0.70866	0.00007	0.97%
MAW4-3	9.4	1526	4.8	0.04	0.01	0.5	623	0.70867	0.00004	1.25%	MAW4-Spot-3	9.4	4.2	0.09	0.02	1.3	1155	0.70870	0.00008	0.95%
MAW4-4	9.9	1585	5.0	0.04	0.01	0.4	925	0.70870	0.00004	1.25%	MAW4-Spot-4	9.9	3.9	0.07	0.02	1.4	1011	0.70873	0.00008	0.88%
MAW4-5	10.4	1600	4.9	0.06	0.01	0.4	1421	0.70870	0.00004	1.26%	MAW4-Spot-5	10.4	4.3	0.08	0.02	1.3	654	0.70874	0.00007	0.45%
MAW4-6	10.9	1560	4.5	0.06	0.01	0.4	149	0.70871	0.00004	1.26%	MAW4-Spot-6	10.9	4.2	0.05	0.01	1.3	1116	0.70874	0.00007	0.49%
MAW4-7	11.4	1595	4.7	0.12	0.02	0.4	552	0.70870	0.00004	1.27%										
MAW4-8	11.9	1458	4.2	0.07	0.02	0.5	624	0.70869	0.00004	1.27%	MAW4-Spot-8	11.9	5.6	0.10	0.02	0.8	609	0.70867	0.00006	1.99%

883

884 **Table 3:** Operating parameters of the NU Plasma MC-ICP-MS and the two laser ablation
885 systems.

886

NU Plasma MC-ICP-MS			
RF Power	1300 W		
Argon cooling gas flow rate	13 L/min		
Auxiliary gas flow rate	0.93 L/min		
Interface cones	Ni		
Lens settings	Optimized for maximum signal intensity and $^{87}Sr/^{86}Sr$ ratio		
Mass resolution	Low		
Mass analyzer pressure	3-5 x 10^{-9} mbar		
Detection system	Nine Faraday collectors and one Ion Counter		
Sampling mode	Time Resolved Analysis		
New Wave UP213 nm Laser ablation system			**NWR Femto 200 Laser ablation system**
Sampling approach	Linescan	Spot	Linescan
Wavelength	213 nm	213 nm	200 nm
Line length	750 µm		750 µm
Ar flow rate	0.65-0.79 L/min	0.68-0.78 L/min	0.77 L/min
He flow rate	0.65-0.81 L/min	0.68-0.78 L/min	0.77 L/min
Pre-Ablation			
Frequency	10 Hz	10 Hz	5 Hz
Translation rate	80 µm/s		60 µm/s
Beam width	100-110 µm	110 µm	65 µm
Ablation			
Frequency	10 Hz	5-10 Hz	25 Hz
Translation rate	5 µm/s		5 µm/s
Beam width	80-100 µm	100 µm	55 µm
Dwell time		120 s	
Fluence	20-30 J/cm^2	20-30 J/cm^2	0.7-0.8 J/cm^2
Data Collection			
Gas background	45 s	45 s	45 s
Sample	145 s	85-115 s	145 s
Integration	0.2 s	0.2 s	0.2 s

887